

# 9 Neotectonics

JOSE CEMBRANO, ALAIN LAVENU, GONZALO YAÑEZ  
(coordinators), RODRIGO RIQUELME, MARCELO GARCÍA,  
GABRIEL GONZÁLEZ & GERARD HÉRAIL

Nazca–South American plate interaction provides a classic example of a subduction-type convergent margin (e.g. Dewey & Bird 1970), in which the continental lithosphere overrides the oceanic plate. Evidence of subduction processes having taken place along the western margin of South America since at least Triassic times has been thoroughly described in the literature (e.g. Mpodozis & Ramos 1989) and elsewhere in this book. Although subduction has been an essentially continuous process along the Andes, its impact on the geological evolution of the continent varies with time and along-strike (e.g. Jordan *et al.* 1983b, 2001). Plate kinematics, the subduction of passive and/or active ridges, fracture zones, plate age at the trench, and climate change have all been invoked as controlling factors for continental plate geological evolution and segmentation (e.g. Jarrard 1986; Gutscher *et al.* 2000b; Yañez *et al.* 2001; Lamb & Davis 2003; Yañez & Cembrano 2004; Sobolev & Babeyko 2005). Figure 9.1 shows the tectonic and morphologic elements that shape the geological evolution of the Andean margin. The tectonic segmentation shown on this figure provides a useful reference for the geological evolution of the Andes.

The Andean mountain chain trends NNE–SSW between latitudes 18°S and 48°S with slight local variations in strike but with significant latitudinal changes in morphotectonic configuration (Fig. 9.1). Between 18°S and 28°S, the Andes consist, from west to east, of the Coastal Cordillera, Central Depression, Precordillera and Western (Main) Cordillera with the Altiplano and Puna to the east. The region between 28°S and 33°S, where the subducting slab is subhorizontal, has no Central Depression or active volcanism, and as a counterpart there are Neogene uplifted blocks of the broken foreland cropping out widely in NW Argentina (Jordan *et al.* 1983b). South of 33°S, the Chilean Andes consist of a Coastal Cordillera, a Central Valley and a Main Cordillera that is called the Patagonian Cordillera south of 39°S (Fig. 9.1). On the outer forearc, the coastline is characterized by Quaternary marine terraces that have been uplifted to over 780 m a.s.l. in Peru (Ortlieb & Macharé 1990).

In northern Chile, the Altiplano and Main Cordillera show the overall highest elevations of the Andes, with mean elevations of 4000 m and some mountains reaching over 6000 m. In contrast, the southern Chilean Andes have an average elevation of 1500 m and only locally reach 4000 m. These gross differences in topography are consistent with a crustal thickness of almost 70 km under the Altiplano and Western Cordillera but only 30 km in the south Andes (Tassara & Yañez 2003).

The main crustal-scale margin-parallel fault zones of the Chilean Andes are the Mesozoic–Cenozoic Atacama Fault System (AFS) in the Coastal Cordillera of northern Chile, the Cenozoic Domeyko Fault System in the Precordillera of northern Chile and the Meso-Cenozoic Liquiñe–Ofqui Fault Zone (LOFZ) in the Main Cordillera of southern Chile. The AFS is the most important tectonic feature of the Chilean forearc, whereas the LOFZ is an intra-arc fault that extends along the margin of the Miocene–Pliocene and present-day volcanic arcs (Fig. 9.1).

In the first part of this chapter the relative importance of plate kinematics and related controlling factors are reviewed. The second part deals with the interplay between Neogene tectonic activity and landscape evolution of the central Andes forearc. Finally, the third and last section examines the stress field within the central and southern Chilean Andes since Pliocene times, using kinematic analysis of neotectonic fault systems.

## Neogene–Quaternary Nazca–South American plate interaction (G.Y.)

### *Late Tertiary plate kinematics*

Nazca (Farallon)–South American plate interaction has been documented in the literature since the mid-1980s, based on analysis of seafloor spreading magnetic anomalies (e.g. Pilger 1983; Pardo-Casas & Molnar 1987; Cande *et al.* 1987; Tebbens & Cande 1997). Recently, Somoza (1998) carried out a new compilation for late Tertiary kinematics of Nazca–South America plate interaction, taking into account all the previous reconstructions and recent information in the Antarctic–Africa–South American area, as well as applying the Nuvel1-A solution for present constraints. Figure 9.2 shows the kinematics of Nazca (Farallon)–South American Plate convergence using the relative poles of rotation of Somoza (1998). Results are computed for the five tectonic segments of the Andean convergence. Some first-order conclusions are clearly displayed in this figure, the most obvious of which is the dramatic change in convergence 25 Ma ago after the break-up of the Farallon Plate. Prior to that time, convergence was relatively slow (*c.* 8 cm/year) and with a large obliquity (*c.* 50°E), favouring the development of dextral strike-slip faulting in the continental plate. Later on, the convergence increased its rate (to more than 14 cm/year), reducing the convergence angle to values in the order of 10–20° (measured counterclockwise from the trench orthogonal). This high rate of convergence between 26 and 10 Ma roughly coincides with an extensional phase recognized in the forearc region of the southern Andes (Jordan *et al.* 2001). High rates of convergence and the development of an extensional regime contradict the common perception that shortening is linked to high convergence rate regimes; this is an important issue which is linked to plate coupling and is discussed later. During the last 20 Ma, convergence rate has decreased steadily from 12 cm/year to values in the order of 7 cm/year over the last 5 Ma (e.g. Somoza 1998, 2005), although the snapshot provided by GPS results (Angermann *et al.* 1999) indicates a present-day value of only 6.3 cm/year (Angermann *et al.* 1999; Kendrick *et al.* 2003). It is important to note that this decrease in the convergence rate is coincident with inversion of the Miocene basin developed during the previous extensional regime (Jordan *et al.* 2001), as well as being approximately coincident with the building of the main Andean mountain chain

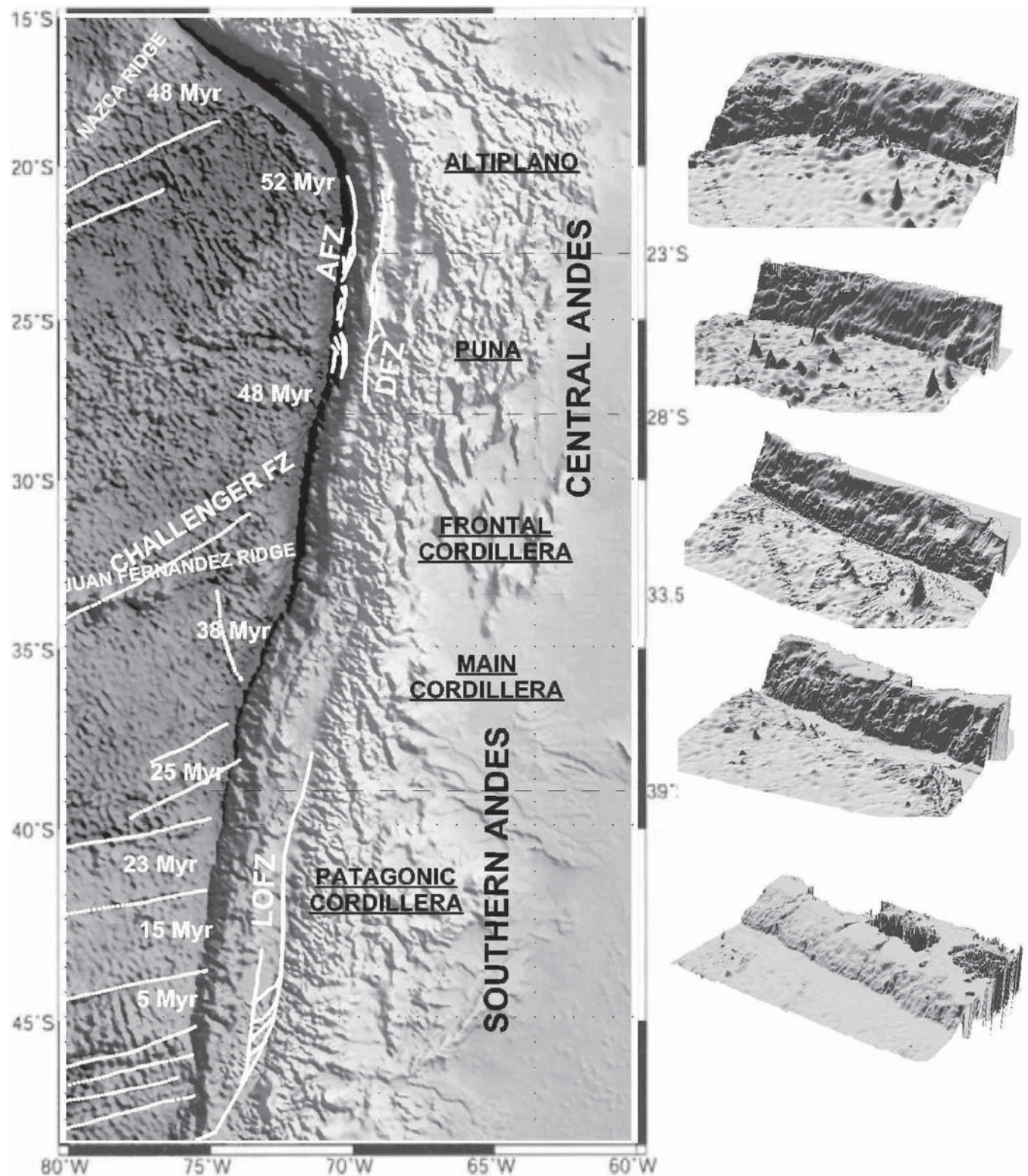


**Fig. 9.1.** Left panel: tectonic framework for the Central and Southern Andes plate boundary zone. Fracture zones, ridges and age of the ocean floor are highlighted for the subducting Nazca Plate. Main tectonic domains of the overriding South American Plate are indicated as are the regional-scale fault zones with Neogene deformation (AFZ, Atacama Fault Zone; DFZ, Domeyko Fault Zone; LOFZ, Liquine-Ofqui Fault Zone). Right panel: bathymetric three-dimensional view of the five segments defined in left panel (DTM model from Zapata 2001). Contour lines on the continental side represent the Benioff plane.

and widespread Pliocene compression. Since 20 Ma, obliquity has remained at low values (*c.* 10–15°), but with some increases between 20 and 15 Ma and within the last 5 Ma (*c.* 20°E). Along-strike variations are second-order features compared to

the general pattern described in the previous paragraphs. One of the most relevant second-order features of the convergence regime is the duration and timing of the high convergence rate period. Whereas in the northern segment it lasted for more than

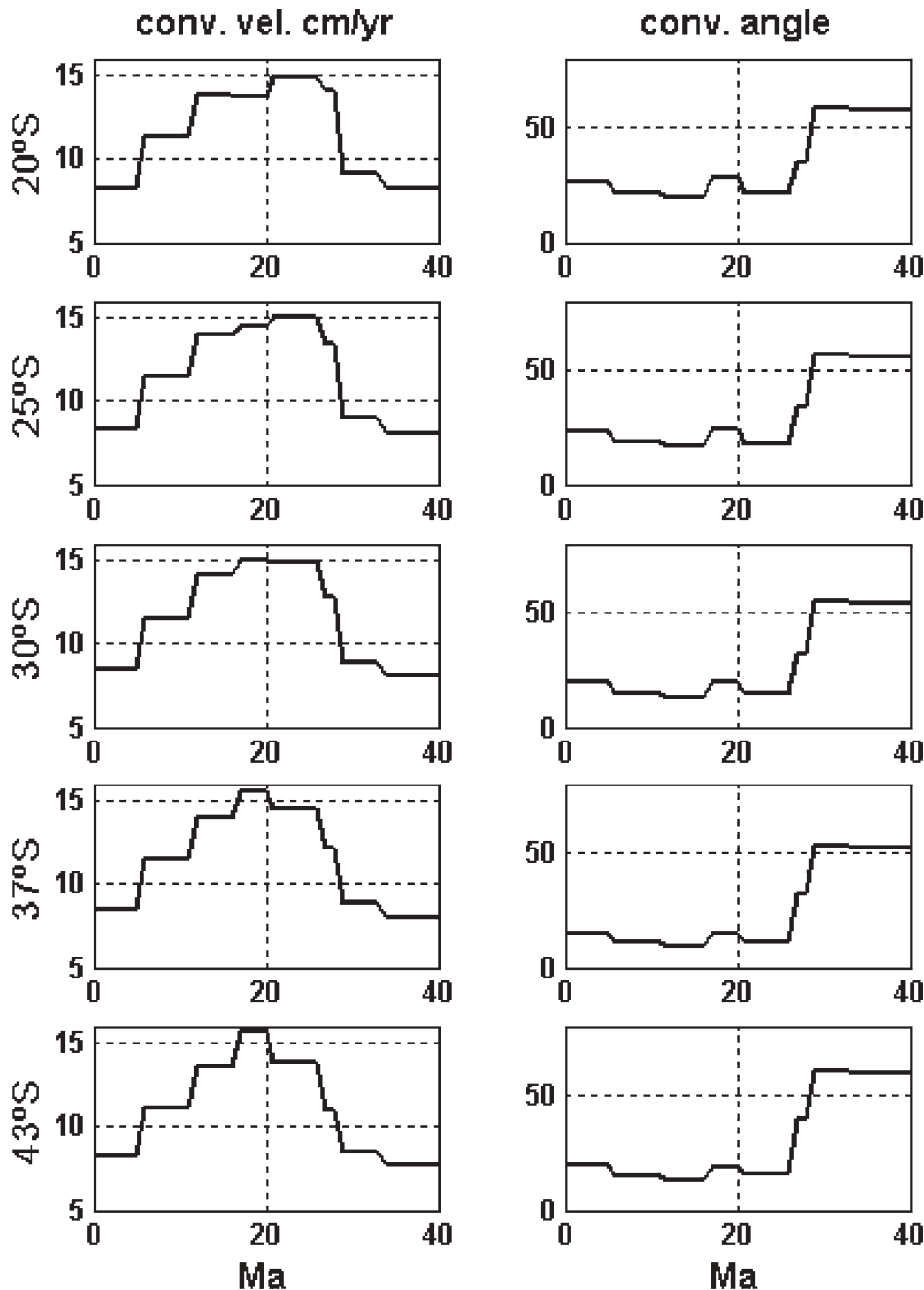


**Fig. 9.2.** Convergence velocity (left panels) and convergence angle (right panels) from Nazca–South American plate reconstruction of Somoza (1998) in the five tectonic segments defined in Figure 9.1. Positive convergence angle represents a dextral movement with respect to the trench strike at each location.

10 million years with a peak at 22 Ma, in the southern region the convergence peak occurred 3 million years earlier, and lasted less than 10 million years. Such a difference can be attributed to along-strike variations of plate coupling and continental lithosphere response.

The role of the Juan Fernandez Ridge in the flattening of the subducting slab has been recently revisited (see for instance Pilger (1981, 1983), Gutscher *et al.* (2000b), Yañez *et al.* (2001, 2002), and elsewhere in this chapter). Flat-slab segmentation explains both the absence of volcanism in the active margin and the transition to a more compressive regime where intrusive bodies are emplaced (e.g. Hollings *et al.* 2003), and deformation

migrates to the foreland region (e.g. Jordan *et al.* 1983b). The kinematics of the Juan Fernandez Ridge during late Tertiary times has been presented in Yañez *et al.* (2001). Figure 9.3 shows a summary of the ridge path during this time period, considering the hot-spot reference frame proposed by Gordon & Jurdy (1986). Although a new plate reconstruction presented by Somoza (1998) incorporates some variations in the plate kinematics (especially within the last 10 million years), the main features of the plate interaction remain the same as represented in the Gordon & Jurdy (1986) model. The collision of the Juan Fernandez Ridge with the South American margin migrated southward at a rate of more than 200 km/Ma during the time



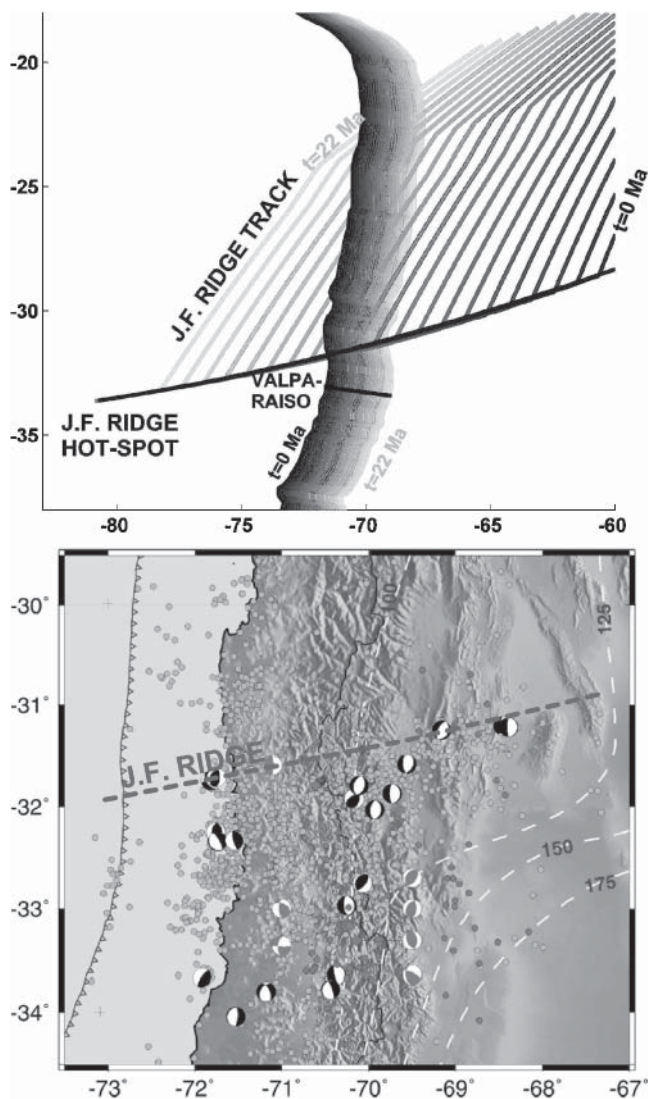


**Fig. 9.3.** Upper panel: predicted track of the Juan Fernandez Ridge in a hot-spot reference frame (rotation poles from Gordon & Jurdy 1986). Lower panel: the trace of the Juan Fernandez Ridge (segmented blue line) over the seismicity of central Chile (modified from Pardo *et al.* 2003b). In the upper panel the time evolution of the Juan Fernandez Ridge and the South American margin are graded from dark (present time) to light (22 Ma before present), with a time interval of 1 Ma. Notice that the South American margin is slowly moving to the west, whereas the track of the Juan Fernandez Ridge is moving towards the east at a much faster rate (at least three times faster). Seismicity in the lower panel is indicated by light dots, and the contours of the Benioff plane by dashed white lines. Notice the good correspondence between the track of the Juan Fernandez Ridge and the cluster of seismicity aligned in the ENE direction. Focal mechanism along this seismic cluster is variable as indicated by some selected events.

period 22–10 Ma. Later on, the ridge collided with the central part of Chile (33°S), roughly coeval with the onset of the flat-slab in this tectonic segment (e.g. Kay & Mpodozis 2002). The trace of the Juan Fernandez Ridge underneath the continent coincides with the projection of the interplate seismicity in the region (Pardo *et al.* 2003b), suggesting a direct link with the ridge morphology (Fig. 9.3). Focal mechanisms obtained by Pardo *et al.* (2003b), suggest processes differing from the classic thrust behaviour of subducting plates. A thicker oceanic crust (e.g. Contreras & Vera 2003) along the ridge probably triggers

seismic expressions of unusual mechanical behaviour including phase transitions and water release from a probably saturated crust. Excessive water release may also be relevant to the anomalous magmatism associated with the source of the Miocene giant copper deposits of the High Andes (e.g. Garrido *et al.* 2002).

#### *Active and passive ridge collision and migration: the connection with the flat-slab segmentation*

Several models have been postulated to explain flat-slab segmentation along active margins (for a review see Gutscher 2002); however, a growing amount of empirical and theoretical evidence (e.g. Yañez *et al.* 2001; Gutscher 2002) suggests a direct link with the larger buoyancy of subducted passive ridges. The subduction of the oceanic plate underneath the continental plate results simply from buoyancy differences, with the density of the subducting slab being mostly controlled by the advection of low temperature isotherms associated with the cooling path of the oceanic plate (e.g. McKenzie 1967). This cooling path is perturbed when a hot-spot generates a volcanic chain that becomes a passive ridge younger and more buoyant than the surrounding plate. However the dip angle of subduction is the result of a delicate equilibrium between the thermally/compositionally controlled negative buoyancy of the subducting slab and the pressure forces associated with the asthenospheric corner flow (e.g. Turcotte & Schubert 2002). The greater buoyancy attributed to the subduction of passive ridges produces both thermal resetting and phase changes with depth. Thermal resetting is a transient phenomenon that depends on the size of the heat source and the time span between the thermal event and the subduction of the ridge. Assuming a linear heat source of 10 km radius, the thermal effect decays to 20% in 6 million years, whereas for a 25 km radius the thermal decay takes more than 40 million years. On the other hand the subducting plate is not uniform mantle pyrolyte but, because of melting at the ridge axis, it has segregated into a basaltic ocean crust (*c.* 5 km thick), and residual harzburgite underlain by ordinary pyrolyte (e.g. Ringwood 1991). According to Ringwood (1991), thermally equilibrated density contrasts, with respect to the reference pyrolyte mantle, are positive in the basaltic layer down to the 650 km discontinuity (200 kg/m<sup>3</sup> in the first 400 km and 50 kg/m<sup>3</sup> in the deeper part), below which it becomes negative (–200 kg/m<sup>3</sup>). On the other hand the depleted harzburgite is less dense than the reference mantle down to 650 km depth (–80 kg/m<sup>3</sup> in the first 400 km and –30 kg/m<sup>3</sup> downwards), and below the 650 km transition zone it is more or less neutral. In consequence, the net buoyancy difference between normal and thicker oceanic lithosphere is determined by the thickness of the basaltic layer and the depleted harzburgite mantle.

The thickness of the basaltic layer underneath the Juan Fernandez Ridge is about 8–10 km (Contreras & Vera 2003), whereas the thickness of the depleted harzburgite mantle below is not well constrained. If we assume a linear relationship with the thickness of the enriched basaltic layer, we can estimate a thickness of at least 50 km for this depleted harzburgite layer (which is normally about 25 km: Ringwood 1991). The net effect on the buoyancy of the subducting plate is a density contrast of –16 kg/m<sup>3</sup> for a 650-km subducting plate of 100 km thickness. In addition, the shape of the Juan Fernandez Ridge (Contreras & Vera 2003) provides a first-order estimate of the heat source size (*c.* 10 km radius). Its effects at the trench have a time lag of 11 Ma (Yañez *et al.* 2001), so that the temperature of the thermally perturbed slab would rise about 10%, producing a density contrast of –5 kg/m<sup>3</sup>. Figure 9.4 shows the theoretical torque associated with the pressure and buoyancy forces as a function of the dip angle for realistic values (see figure captions for details). Both competing effects decay as the slab becomes

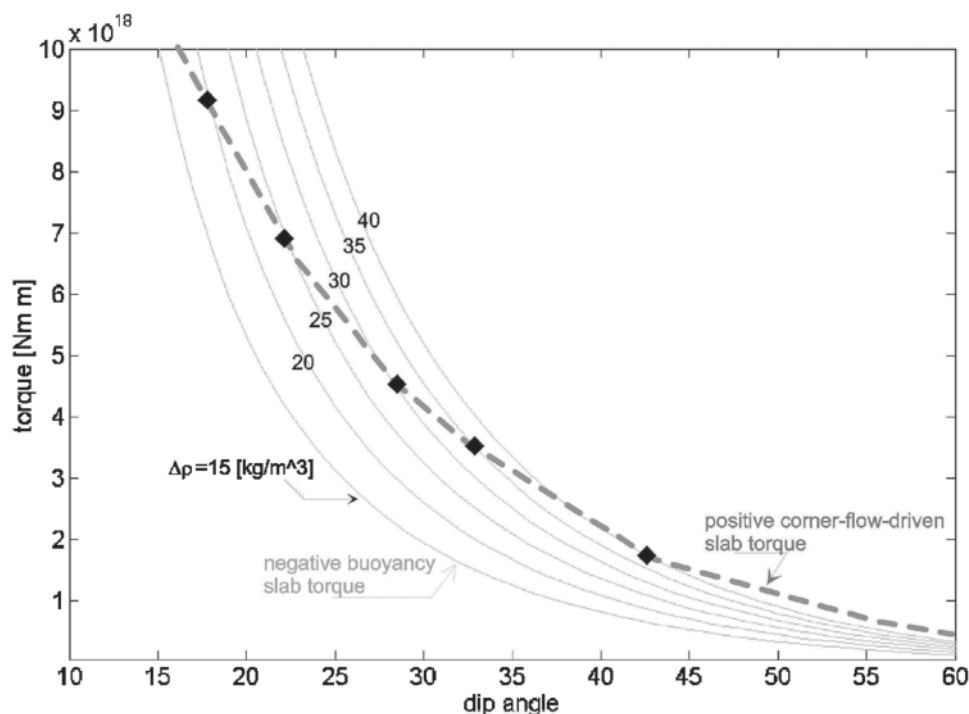


**Fig. 9.4.** Absolute values of the positive corner-flow-driven slab torque (thick dashed line), and negative-buoyancy slab torque (continuous thin lines for different density contrasts). The 'negative' pressure field that controls the corner-flow-driven slab torque is computed using finite elements scaled by an asthenosphere viscosity of  $10^{20}$  Pa s and a convergence velocity of 8 cm/year. The thermally buoyant slab is a 50-km-thick layer with a variable length along-strike (depending on the dip angle). Diamonds represent the equilibrium points for a given density contrast. For larger dip angles the pressure field dominates, forcing a reduction in the dip angle. Eventually, if the density contrast is too small the pressure field will force an almost  $0^\circ$  dip angle (i.e. for a density contrast of  $15 \text{ kg/m}^3$  in the present exercise).

vertical, although when the density contrast is larger the negative buoyancy torque is consistently much greater. An equilibrium condition is achieved for progressively smaller dip angles when the density contrast is being reduced. Focusing on the Juan Fernandez Ridge, the semi-quantitative result of Figure 9.4 indicates that a reduction of the order of  $-21 \text{ kg/m}^3$  reduces the net buoyancy by more than 40%, this in turn inducing a reduction in the dip angle of  $15\text{--}20^\circ$ .

The path of the Juan Fernandez Ridge during the last 20 million years, shown in Figure 9.3, predicts a southward migration of the flat-slab during this period. Present evidence for the presence of the Juan Fernandez Ridge is recorded in the anomalous seismicity pattern along the track of the ridge underneath the continent (Fig. 9.3). Focal mechanisms from Pardo *et al.* (2003b) suggest a complex interaction with the upper plate and metamorphic effects linked with water release as the subducted plate heats up. Geological evidence (Kay & Mpodozis 2002) consistently shows that magmatism related to flat-slab subduction migrates southward with the same timing as that of the Juan Fernandez Ridge path. It may be concluded, therefore, that flat-slab segmentation is a transient phenomenon that depends on the anomalously enhanced thickness of subducted oceanic crust, and on the associated release of heat.

#### *The role of plate coupling in the build-up of the Andes*

Two different hypotheses have recently been presented to explain the role of plate coupling on Andean orogenesis. Yañez & Cembrano (2004) postulate that plate coupling is mostly controlled by the age of the oceanic plate and only secondarily by convergence velocity. Stronger coupling is achieved for older (cooler) plates and slower convergence regimes. On the other hand, Lamb & Davis (2003) predict that sediment fill reduces the shear stress at the trench, weakening plate coupling, but

increasing the down-dip extent of the coupling zone. In this latter model, late Cenozoic changes in sediment fill linked to climate change triggered the uplift of the Andes. Both effects successfully explain the uplift of the Altiplano region in the last 20 Ma, and both are probably reinforcing the other where older oceanic crust and the sediment-starved trench are spatially coincident (Fig. 9.5). However, it is argued here that, as a general mechanism, the climate hypothesis has some limitations, notably that it is not relevant to pre-late Cenozoic time. Prior to the opening of the Drake Passage (late middle Eocene–early Miocene) climate conditions in the western margin of South America ranged from tropical rainforest and paratropical rainforest to woodland (Frakes *et al.* 1992). Also, given the fact that present relief is a first-order expression of plate coupling, the rather gradual southward reduction of relief contrasts with the sharp reduction of trench fill to the north of  $33^\circ\text{S}$  (see in Fig. 9.1 the transition between a deep trench to the north of this latitude). In addition, tectonic erosion processes carry a large amount of sediment downwards, in almost the same fashion as filled trench environments (C. R. Ranero, pers. comm., 2005). Plate coupling, mainly controlled by the age of the oceanic plate and the convergence velocity, also provides a reasonable explanation for the apparently contradictory nature of the plate kinematics previously mentioned: higher compressive regime when the convergence rate is lower and vice versa. Higher convergence velocity decreases the age of subducted crust at the trench and also reduces the effective viscosity at the slip zone (given a power law rheology at the plate contact zone), reinforcing a reduction in plate coupling. The opposite is consistently true for slowing the convergence velocity, which enhances higher coupling. A sharp transition in the plate coupling is predicted across offset fracture zones of great age, such as the Challenger Fracture Zone in Central Chile (Fig. 9.1). In this

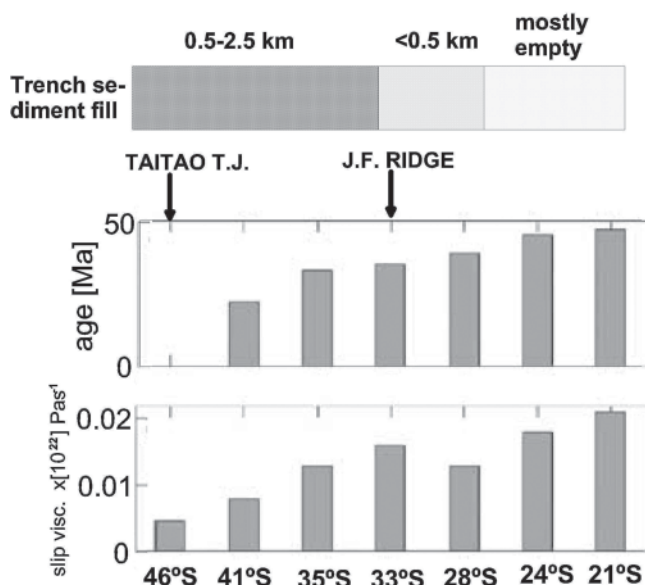


**Fig. 9.5.** Correlation between the ages at the trench (middle panel) with the trench fill (upper panel) and the viscous plate coupling (lower panel), extracted from Lamb & Davis (2003), and Yañez & Cembrano (2004), respectively. The viscous plate coupling is expressed in terms of the slip viscosity at the plate contact.

case the model predicts the occurrence of *c.* east–west trending deformation zones in the overriding plate that accommodate the deformation, expressed for example as the Melipilla Fault Zone at the latitude of Valparaíso (33.5°S) (Yañez *et al.* 2002), and the origin of at least some of these can be linked to this differential coupling across fracture zones offsetting oceanic crust with markedly differing age.

### Discussion

Nazca–South America plate interaction during late Tertiary times has had a fundamental impact on the geological evolution of the active margin of South America, with transient events modulating the long-lived continuous activity of the subduction factory. Long-term geological effects on the overriding plate are probably controlled by pre-existing heterogeneities on a lithospheric scale (e.g. Tassara & Yañez 2003); these regulate the way in which the continental plate accommodates the deformation forced by the tectonic boundary conditions. Key elements in the stress regime at the continental lithosphere margin are absolute plate velocities, plate coupling and subduction of buoyant slabs (e.g. Yañez & Cembrano 2004; Sobolev & Babeyko 2005). All these parameters are inherently variable and episodic with time and space. A good example of this episodicity is shown in the evolution of the Nazca (Farallon) Plate during late Tertiary times. Prior to the break-up of the Farallon Plate (25 Ma) the oceanic plate was moving in a NE direction, producing highly oblique convergence at the plate margin. With the plate moving NE, the presence of the Juan Fernandez hot-spot in the middle of the Pacific generated a volcanic chain aligned in the same direction. After the break-up of the Farallon Plate, however, a new regime was established with a much faster and highly oblique convergence. This abrupt change resulted in the subduction of the Juan Fernandez Ridge underneath the continent and the arrival of progressively younger (and hotter) oceanic crust at the South American trench. Subduction of more buoyant oceanic lithosphere allowed the generation of a flat-slab segment that migrates southward, following the path of the thermally and compositionally perturbed subducted slab. Plate segmentation by the flat-slab has had a pronounced effect on the geological

evolution of the continental margin. In the flat-slab segment the reduction of the asthenospheric wedge induces an eastward migration of the volcanism and the deformation front. Such tectonomagmatic events probably favoured the development of the giant late Miocene ore deposits of the main Cordillera (Garrido *et al.* 2002). The much faster convergence rate and the arrival of younger oceanic crust at the trench also reduces the coupling between plates (Yañez & Cembrano 2004), enhancing the development of an extensional regime in the forearc region and therefore the accumulation of a thick pile of sediments (i.e. Abanico Formation). Reduction in the plate convergence in the last 10 million years induced the opposite effect in plate coupling, with progressively older oceanic crust at the trench and lower strain rate at the slip layer. This new tectonic boundary condition generated the inversion of the previously developed basin and regional uplift of the Andes.

The generalized description of late Tertiary Nazca (Farallon)–South American plate interaction outlined in the previous paragraph emphasizes the relevance of episodic events in the geological evolution of the continental margin. Thus, from 40 to 25 Ma there was a highly oblique convergence at a rate of *c.* 8 cm/year, then a more orthogonal and higher convergence rate of 14 cm/year (25–15 Ma), and finally a slowdown in convergence velocity to 7 cm/year (<12 Ma). Such transient events are mostly controlled by heterogeneities and kinematic changes in the oceanic plate. The geological record in the Andean evolution is in fact plagued by episodic events restricted in time and space. For instance, the episodic slowdown in plate convergence rates since 20 Ma is clearly coeval with discrete shortening events of the Andes build-up, as will be documented in the following sections.

### Neogene tectonic activity and landscape evolution of the central Andes forearc, northern Chile (R.R., M.G., G.G. & G.H.)

This section examines Neogene tectonic activity in northern Chile, between 18°S and 28°S, and its relation to the present-day landforms. This region is emphasized specifically because it has remarkable and well exposed examples of interactions between tectonic activity and morphogenesis. Exceptional preservation and exposure of the landscape has been made possible due to the arid to hyperarid climatic conditions in the region which have prevailed at least since middle Miocene times (Sillitoe & McKee 1996; Alpers & Brimhall 1988, 1989; Hartley & Chong 2002). The Neogene tectonic activity of the region has been studied through analysis of landscape evolution, although the exact nature of the deformation mechanisms operating in the forearc and arc during the Neogene is still far from being fully understood. However, there is no doubt that relating tectonics to geomorphological evolution has the potential to better constrain the deformation history and give new insights into recent regional deformation mechanisms of northern Chile.

#### Geomorphological and geological setting

In the forearc region of northern Chile, between the latitudes of Arica (18°S) and Copiapó (28°S), five north–south elongated physiographic units can be differentiated. These units are, from west to east, the Coastal Cordillera, the Central Depression, the Precordillera, the Preandean Depression and the Western Cordillera (Fig. 9.6). The geological record of these physiographic units shows eastward migration of a subduction-related magmatic arc from the Jurassic period to the present. The present-day position of the magmatic arc in the Western Cordillera was reached about 25 Ma (e.g. Coira *et al.* 1982). The Mesozoic to Cenozoic migration of the magmatic arc has



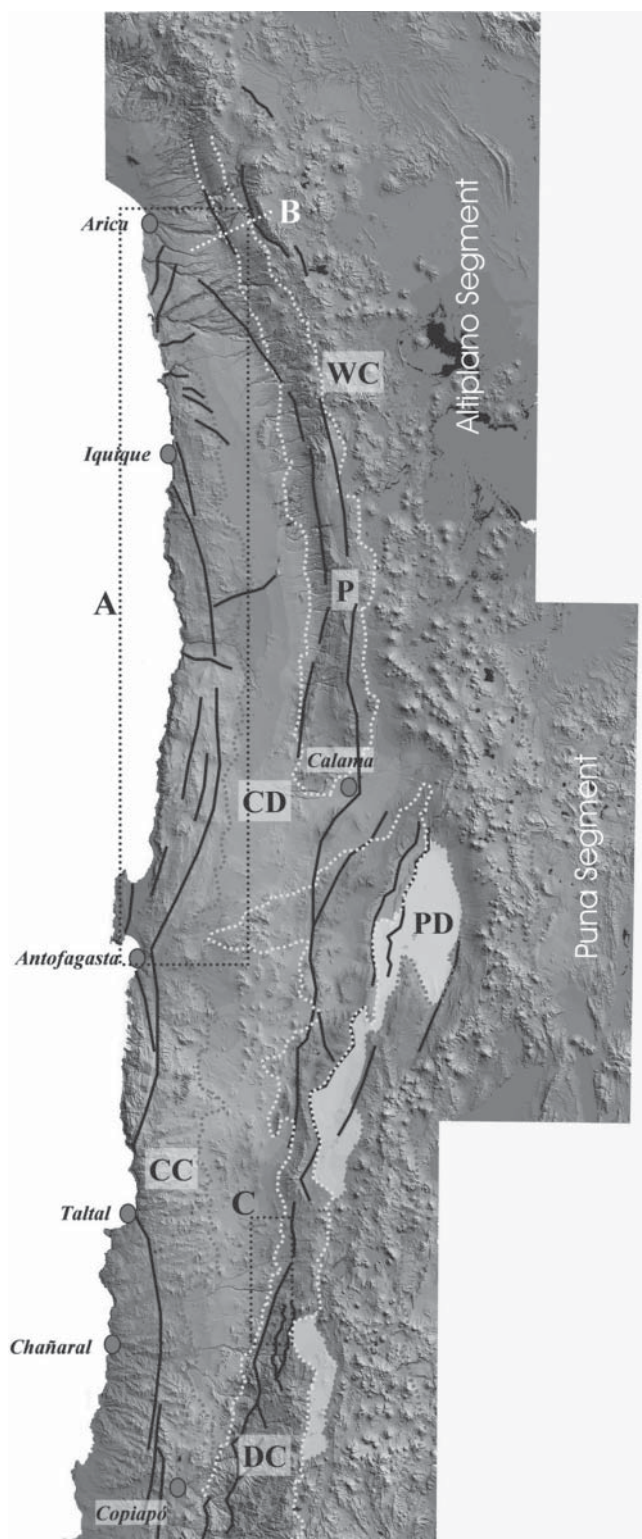


**Fig. 9.6.** Location and physiographic units of northern Chile: CC, Coastal Cordillera; CD, Central Depression; DC, Domeyko Cordillera; P, Precordillera; PD, Preandean Depression; WC, Western Cordillera. The main fault systems of the forearc region are shown: the Atacama Fault System (AFS) in the Coastal Cordillera and Domeyko Fault System (DFS) in the Precordillera and Domeyko Cordillera. Locations of Figures 9.8 (A), 9.9 (B) and 9.11 (C) are indicated.

been accompanied by the development of two north-south orientated megafault systems (e.g. Scheuber & Reutter 1992): the Atacama Fault System, located in the Coastal Cordillera, and the Domeyko Fault System, located in the Precordillera

(Maksaev 1990; Reutter *et al.* 1996) (Fig. 9.6). In addition to the movement accommodated by these two megafault systems, clockwise rotation around a vertical axis linked to the formation of the Bolivian Orocline has been recorded in the forearc region by palaeo-magnetometry (e.g. Arriagada *et al.* 2000). The two major longitudinal segments of the central Andes east of the Western Cordillera are the Altiplano and Puna (Fig. 9.6). These regions represent two different Cenozoic geological domains that can be distinguished on the basis of their deformation styles and lithospheric composition (Whitman *et al.* 1992, 1996; Tassara & Yañez, 2003; Allmendinger *et al.* 1997). Similar and corresponding first-order variations also seem to be reflected in the arc and forearc regions.

#### *Coastal Cordillera*

This can be traced for more than 1000 km along-strike between 18°S and 28°S. The average elevation is about 1500 m a.s.l., reaching a maximal elevation of 2700 m a.s.l. The western flank of the Coastal Cordillera is formed by a prominent and continuous coastal cliff of 1000 m average height and a maximum relief up to 2000 m (Mortimer *et al.* 1974). The main structural system of the Coastal Cordillera is the Atacama Fault System (AFS) which is located in the inner part of the range (Fig. 9.6). In contrast to its western flank, the topographic transition between the Coastal Cordillera and the Central Depression is smooth and much less abrupt.

#### *Central Depression*

Between 18°S and 23°S, this is a relatively smooth and flat surface with average altitude of 1500 m a.s.l. This flat surface represents the top of a Neogene infill, composed of rhyolitic tuff and continental sedimentary deposits, that together reach a stratigraphic thickness of up to 1000 m. South of Antofagasta, at 23°S, the flat surface of the Central Depression is interrupted by topography characterized by isolated hills and ranges (monadnocks) that rise over an undulating surface formed by coalescent and overlapping alluvial fans. These alluvial fans represent the final stages of the Neogene infill which in this region does not surpass 500 m in thickness (Riquelme 2003). The elevation of this portion of the Central Depression varies from 1200 to 2000 m a.s.l.

#### *Precordillera*

This is a prominent positive morphostructure that can be followed between 18°S and 22°30'S reaching altitudes between 3500 and 4500 m. Contrasting morphological, geological and structural features allow the subdivision of this morphostructural unit into two segments: a northern segment (18°S to 22°30'S) referred in the geological literature only as Precordillera (e.g. Muñoz & Charrier 1996), and a southern segment (22°30'S to 27°30'S) indistinctly called the Precordillera or Cordillera de Domeyko (e.g. Mpodozis & Ramos 1989). In this text, for the sake of clarity, we will refer to this geomorphological unit as the Precordillera for the northern segment and the Cordillera de Domeyko for the southern one. The Precordillera forms the piedmont of the Western Cordillera. The northern and highest part of the Precordillera is covered by Miocene ignimbrites which are affected by west-vergent monoclinical folding. Along its southern extension, in the highest part of the Precordillera, deep structural levels represented by a basement of Palaeozoic sedimentary and igneous rocks are exposed and thrust over Jurassic and early Cretaceous sedimentary units. Further south, the general structural framework of the Cordillera de Domeyko is dominated by an anastomosing north-south trending fault system linked by strike-slip and reverse faults, the Domeyko Fault System (DFS). The highest parts of the Cordillera de Domeyko are formed by late Palaeozoic igneous and volcanic rocks (e.g. Mpodozis & Ramos 1989). The Cordillera Domeyko borders an intermontane basin, the Preandean Depression, to the east (Fig. 9.6). This basin has an elevation of 2500 to 3000 m and contains the major Atacama, Punta Negra and Pedernales salars.

### Western Cordillera

In northern Chile the Western Cordillera is dominated by a continuous Neogene volcanic chain which reaches elevations of up to 6893 m a.s.l. (Ojos del Salado stratovolcano). It forms the western border of the Bolivian Altiplano basin which lies at 3800–4200 m a.s.l. Between 18°S and 19°30'S, the Neogene volcanoes overlie deformed Oligocene–early Miocene volcanic and sedimentary rocks (Salas *et al.* 1966; Lahsen 1982; García 2001), which themselves unconformably cover Proterozoic–Palaeozoic metamorphic basement in the Belén area.

### Neogene structural framework

The recent fault scarps of the northern Chilean forearc and arc are best exposed along the Coastal Cordillera, in contrast to most of the other parts of the region which are characterized instead by poor geomorphological expressions of underlying faults. An exception is provided by the topographic boundary region between the Precordillera and Central Depression which is controlled by broad, open folds affecting the Oligocene–Miocene strata.

### Neogene structures of the Coastal Cordillera

The geomorphology of the Coastal Cordillera is characterized by prominent, fault-related topographic features (Fig. 9.7)

which offset a 20–14 million-year-old mature planar surface at the top of the range (Dunai *et al.* 2005). The most significant structures of the Coastal Cordillera are north–south trending faults and lineaments, grouped within the AFS (Arabasz 1971; Brown *et al.* 1993). Other locally important structures include a group of nearly east–west striking reverse faults exposed along the Coastal Cordillera between Quebrada Camarones and Rio Loa (Fig. 9.8) valley (Allmendinger *et al.* 2005).

The AFS extends over 1000 km along the continental margin from south of Iquique (21°S) to La Serena in the south (29°45'S; Fig. 9.6). It has been divided into the Salar del Carmen, Paposo and Salado segments (Naranjo 1987; Thiele & Pincheira 1987) (Fig. 9.6). The earliest movement along the AFS has been constrained to Jurassic to Early Cretaceous times, contemporaneous with arc magmatism in the Coastal Cordillera (Naranjo & Puig 1984; Hervé 1987b; Scheuber & Andriessen 1990; Marinovic *et al.* 1995; Scheuber & González 1999). The most recent activity of the AFS is expressed by large fault scarps that deform the surface of the Coastal Cordillera in the Salar del Carmen and Paposo segments (González & Carrizo 2003; Fig. 9.7B,C). However, farther to the south, in the Salado Segment, the youngest tectonic activity does not form fault scarps, but is expressed by a sharp geomorphological contrast between both sides of the AFS (Riquelme *et al.* 2003).

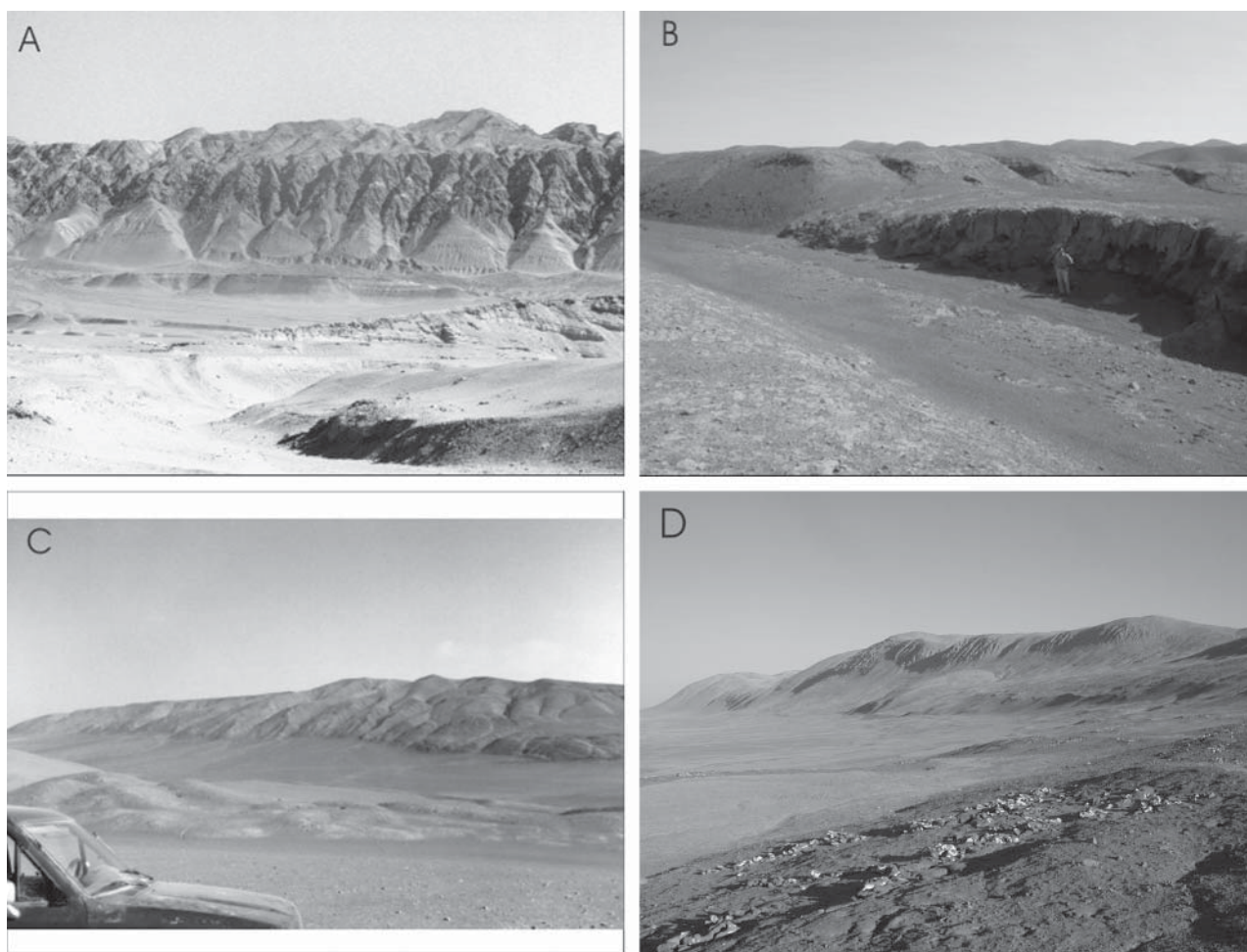


**Fig. 9.7.** Fault scarp related to normal faults of the outer forearc. (A) Flat iron formed in Plio-Pleistocene marine sediment of the Mejillones Peninsula. Country rock formed by Palaeozoic metamorphic rock is in fault contact with Mio-Pliocene sedimentary rocks. Small scarp along the foot of the flat iron is related to a reverse fault connected with normal faulting and backward tilting of the sedimentary cover. View looking to the west. (B) Fault scarp formed by the reactivation of the Atacama Fault System near Antofagasta. View looking to the NW. (C) Fault in line scarp of the Atacama Fault System close to Salar Grande Area. View looking to the NE. (D) Reverse, east–west orientated fault scarp, 300 m high, showing the spectacular deformation of the Miocene topography of the Coastal Cordillera east of the Salar Grande.



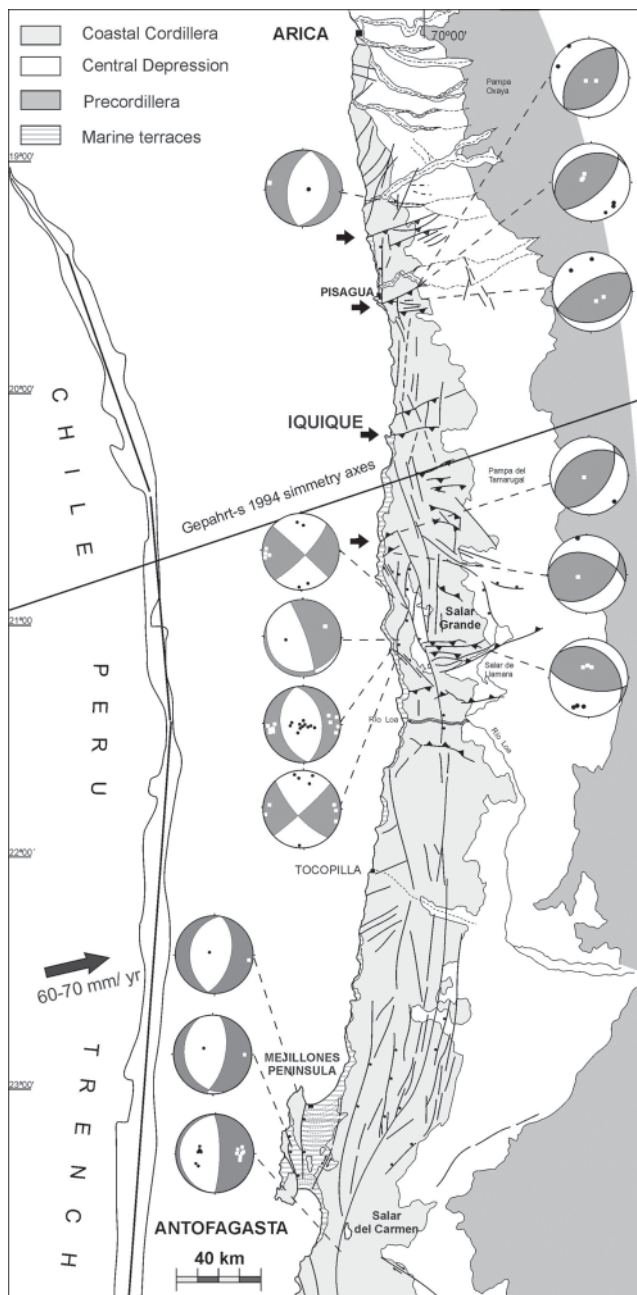


**Fig. 9.8.** Structural map of the central Andes forearc in northern Chile. Stereographic diagrams show a summary of fault kinematic data represented as fault plane solution using the graphical reconstruction of Marrett & Allmendinger (1990). In this diagram white and grey areas correspond to contractional and extensional quadrants respectively. Gephart's symmetry axes of the Bolivian Orocline is represented to show the bilateral symmetry between the occurrence of reverse fault and the position of this axes.

In the Paposo and Salar del Carmen segments, Neogene tectonic activity has disrupted the morphology and produced spectacular fault scarps (Arabasz 1971; Okada 1971; Mortimer 1980; Naranjo 1987; Hervé 1987a; Armijo & Thiele 1990; Delouis *et al.* 1998; González *et al.* 2003) (Fig. 9.7). Most of these authors suggest a predominantly normal movement with a dominant vertical component that has been responsible for the relative uplift of the western side of the AFS. According to the kinematics of some faults along the Salar del Carmen segment, the near-surface strain field is characterized by east–west extension (Delouis *et al.* 1998; González *et al.* 2003) (Fig. 9.8). This extension shows a spectacular expression in

the Peninsula de Mejillones area, where north–south striking normal faults offset Miocene to Pleistocene marine deposits (Armijo & Thiele 1990). In this area vertical displacement varies between 300 and 600 m. Other normal faults are exposed in the northern extreme of the Coastal Cordillera near the town of Pisagua where several normal faults offset Neogene ignimbrites (Allmendinger *et al.* 2005).

The uplift of the western block of the AFS in the Paposo Segment resulted in the tectonic capture of east-to-west directed valleys (Naranjo 1987; Hervé 1987a). In the Salado Segment of the AFS, Neogene vertical slip has cut off the westward flowing rivers, denying them access to the Pacific. The generation of such closed basins east of the AFS has allowed the deposition of >300 m of middle–upper Miocene sedimentary deposits known as the ‘Atacama Gravels’ (Riquelme *et al.* 2003). Both large-scale and local studies of drainage system morphometry have revealed a more incised landscape to the west of the AFS. This situation has been interpreted as evidence for uplift of the western block along the AFS, at least from the mid-Miocene onwards (Riquelme *et al.* 2003).

The approximately east–west trending faults have recently been described by Allmendinger *et al.* (2003, 2005). These structures are expressed as prominent (up to 500 m high) fault scarps, which represent high angle (70° dip) reverse faults (Figs 9.7D & 9.8). Because the reverse faults offset a 15–10 Ma erosional surface of the Coastal Cordillera, the age of the faulting has been constrained as post-mid-Miocene.  $^{40}\text{Ar}/^{39}\text{Ar}$  dating of tuffs intercalated in sediment deformed by the reverse faults indicates that these structures have been reactivated in Pliocene time (Allmendinger *et al.* 2005). Some of these structures offset Late Pleistocene (100–200 ka) marine terraces of the Coastal Cordillera (Caleta Chica, Pisagua, Barranco Alto areas) indicating that the deformation was active as late as the Pleistocene or Holocene.

#### *Neogene structures of the Central Depression and Precordillera (Altiplano segment)*

Neogene tectonic activity near Arica is represented mostly by west-verging gentle folds and high-angle reverse faults. These structures affect Oligocene–Miocene ignimbrites and clastic deposits (Fig. 9.9). The most significant structure in the Precordillera in this region consists of a north–south to N40W-striking fold (Oxaya Anticline; Salas *et al.* 1966; Muñoz & Charrier 1996; García 2002), with an axis extending over 50 km strike length, and wavelength reaching up to 30 km (Fig. 9.9B). This structure has been interpreted as related to the Neogene gravitational collapse of the Western Cordillera (Wörner *et al.* 2000b). However, field observations indicate that it results from the upward propagation of the Ausipar Fault during a relatively short-lived reactivation interval in late Miocene times (12–10 Ma; García 2001; García & Hérail 2005). Across this fold the topography shows a difference in height of about 1500 m between western lowland and eastern highland. The amount of shortening, as determined by balanced cross-section methods, is *c.* 100 m which requires that the Ausipar Reverse Fault must be interpreted as a high angle structure at depth (Fig. 9.9B). Below the 26–19 Ma Oxaya Formation, the Ausipar fault has displaced a Mesozoic folded sequence over Oligocene subhorizontal strata, indicating tectonic activity prior to the folding responsible for the most recent uplift of the Precordillera.

In the Central Depression, around Camarones Valley, a 30-km-long, NW-striking monoclinical flexure deforms the Neogene infill, and has uplifted the eastern block 500 m relative to the western block. This monocline results from the propagation of a NW-striking, east-dipping (50–60°) reverse fault (García 2001). To the south, two monoclinical flexures are exposed around Moquella (Pinto 1999; Pinto *et al.* 2004b) and Aroma (Fariás 2003; Fariás *et al.* 2005b). These structures show a left-stepping, growth strata geometry and form the contact between the Central Depression and the Precordillera.

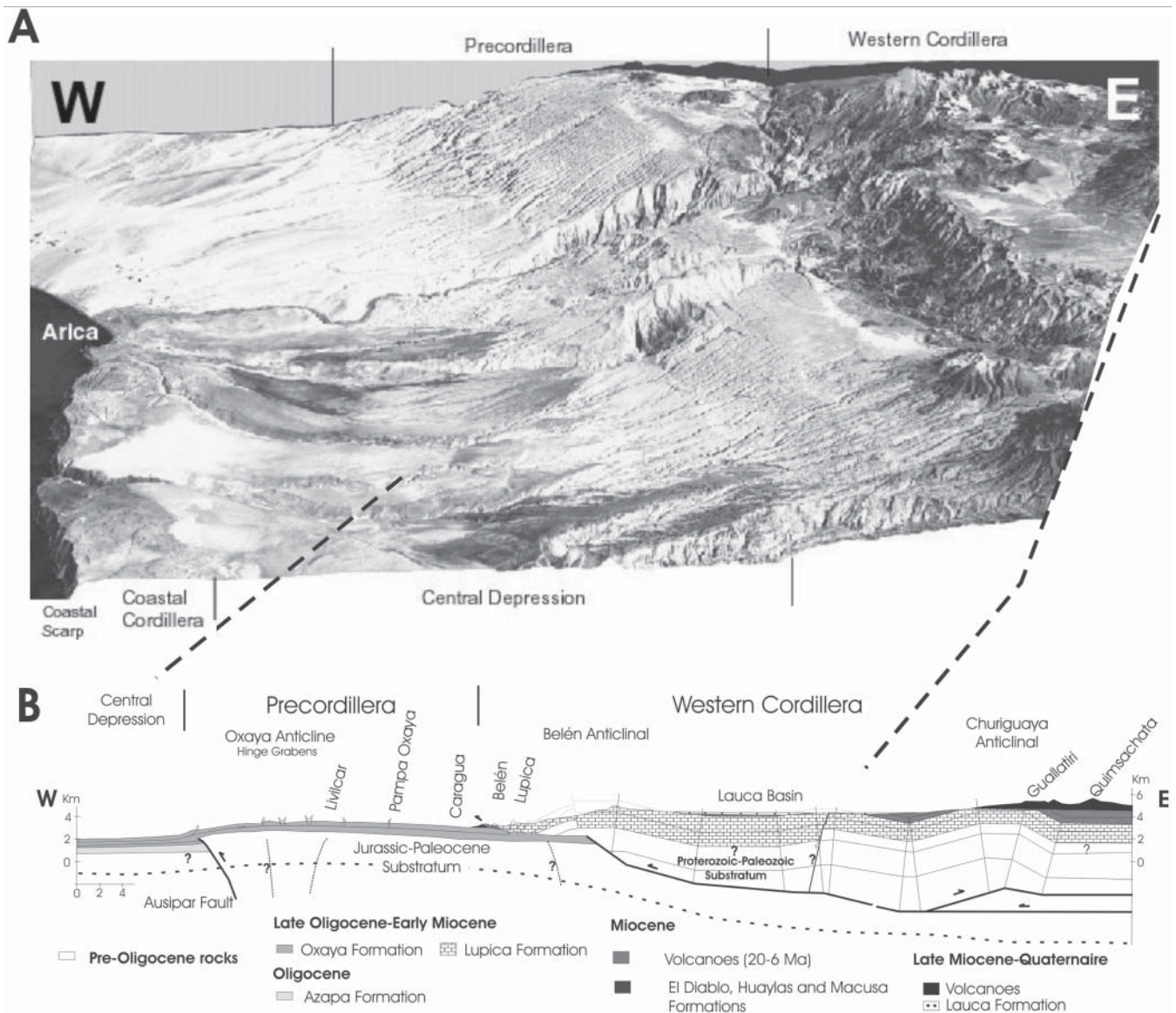


**Fig. 9.9.** (A) Block diagram showing topographical and geomorphological features of the northernmost Andes of Chile, at the latitude of Arica. The figure was constructed overlapping 100 m resolution digital elevation model and Landsat 741 TM5 satellite image. Approximate vertical exaggeration is four times. (B) Balanced cross-section of the Precordillera and Western Cordillera of northern Chile, east Arica, showing two different styles of Neogene west-vergent basement-involving folding and faulting (García 2001).

East of the Iquique and Pica area (20°30'S), between the Precordillera and Central Depression, the topography shows a major step of 2500 m due to another major monoclinical flexure (Galli & Dingman 1962; Victor *et al.* 2004). South of Pica, the boundary between the Precordillera and Central Depression is represented by a system of east-dipping reverse faults that uplift basement blocks of the Sierra de Moreno. Movement on this fault system has largely been constrained to the Mesozoic to early Cenozoic (Skarmeta & Marinovic 1981). However, movements accommodated by some of these faults cut or gently fold Miocene strata and indicate minor Neogene reactivation. Similar minor Neogene faulting has also been documented on the eastern border of the Sierra de Moreno (Reutter *et al.* 1996).

#### *Neogene structures of the Cordillera de Domeyko (Puna segment)*

Much of the tectonic configuration of the Domeyko Cordillera is controlled by the north-south trending Domeyko Fault

System (Fig. 9.6). This structure results from a thick-skinned uplift of a late Palaeozoic plutonic and volcanic basement that is bounded by a system of reverse faults and folds, whose vergence alternates along-strike (Coira *et al.* 1982; Reutter & Scheuber 1988; Mpodozis & Ramos 1989). Reverse faults and folds affect a Late Cretaceous–Miocene cover and have resulted in the inversion of a Mesozoic backarc marginal basin since middle Cretaceous times (Muñoz *et al.* 2000, 2002). The Cenozoic timing and kinematics of the structures related to the DFS are poorly constrained; however, it was active during the lifespan of the Eocene to early Oligocene magmatic arc, showing both important strike-slip movement as well as shortening (e.g. Reutter *et al.* 1991, 1996; Tomlinson & Blanco 1997; Niemeyer 1999). Both eastern and western foothills of the Domeyko Cordillera are mainly composed of extensive alluvial fan sediments and pedimentation-related deposits accumulated from middle-late Miocene times to the present day (Sáez *et al.* 1999; Kober *et al.* 2002; Riquelme 2003). Active faulting and



folding attributed to the Neogene reactivation of DFS structures has been reported in the eastern and western flank of the Domeyko Cordillera. Neogene faulting has been documented to the east, in the Salar de Atacama area (e.g. Jolley *et al.* 1990; Flint *et al.* 1993; Mpodozis & Clavero 2000; Muñoz *et al.* 2000, 2002; Jordan *et al.* 2002) (Fig. 9.10). On this flank, intermittent local uplift due to thrust tip propagation controls the Neogene topographical and sedimentological evolution. The appearance of a distinctive series of discrete sub-basins (e.g. Llano la Paciencia and Pampa Viscachita), as well as eastward progradation of alluvial fans, both result from the activity of an east-vergent thrust system. The Cordillera de la Sal is an intrabasinal physiographic unit running down the eastern border of the Atacama Salar. It has been interpreted as a thin-skinned contractional feature folding and thrusting a Mio-Pliocene sedimentary sequence some 2000 m thick (Flint *et al.* 1993) (Fig. 9.10). West-dipping blind thrusting in the Atacama Salar represents the youngest tectonic activity in this area (Jordan *et al.* 2002). Active faulting and folding occur without topographic expression, and net reverse offset across the faults, which can reach up to 700 m during Pliocene to Recent times, decreases to the east (Jordan *et al.* 2002). Late Miocene to Recent reactivation of DFS-related structures, evident from fault scarps, has recently been reported in the Salar de Punta Negra area (Soto *et al.* 2005).

Around the latitude of Antofagasta (23°S), Neogene strike-slip activity on the eastern side of the Domeyko Cordillera has been reported (Reutter *et al.* 1996; May *et al.* 1999). In contrast, further south Plio-Quaternary tectonic activity without significant strike-slip movements has been recorded on the western flanks of the Domeyko Cordillera and in the westernmost part of the Central Depression (25°30'S and 26°30'S; Audin *et al.* 2003) (Fig. 9.11). These latter authors observed that the relief of these more southerly areas results from north–south trending active vertical faults in the topographically higher pampas

(western flank of the Domeyko Cordillera), and active folding around a north–south trending axis in the lower pampas. In the higher pampas the fault scarps cut through alluvial deposits and are distributed parallel to older tectonic structures (Fig. 9.11). Major vertical, and in some cases composite escarpments, up to 5–10 m high, can be recognized on the northern prolongation of the Sierra Castillo Fault, a main fault of the DFS at this latitude (Fig. 9.11). The dip direction of these escarpments does not change along-strike. Audin *et al.* (2003) identified no strike-slip movement and proposed that the vertical throw could be associated either with normal faults or with overturned thrusts deflecting along bedding planes and showing a normal sense of displacement.

#### *Neogene structures of the Western Cordillera*

Structures affecting the Neogene sequences in the Western Cordillera are best exposed to the east of Arica where north–south to NNW–SSE structures form a complex fold and thrust belt. This belt affects the late Oligocene–middle Miocene rocks of the Lupica, Chucal, Macusa, Joracane and Putani formations, all of which are partially, progressively and unconformably covered by late Miocene–Holocene volcanic and sedimentary rocks (Muñoz & Charrier 1996; García 2001). In the Visviri, Colpitas, Churiguaya and Chucal areas, the deformation is east-vergent, whereas in the Putre–Belén area the vergence is to the west (Fig. 9.9B). In the region of Churiguaya a gentle growth-anticline is exposed, with the anticlinal flanks dipping less than 35°, and with a wavelength of around 20 km. In the Putre–Belén area, Neogene folds and thrusts produce the greatest change of altitude in the region, from an average of c. 3200 m to the west up to c. 5300 m in the east, across a horizontal distance of only 15 km (Fig. 9.9B). In these areas, the Lupica Fm is folded into anticlines and synclines that are thrust to the west over the subhorizontal sequences of the Oxaya and Huaylas formations and middle Miocene volcanic rocks

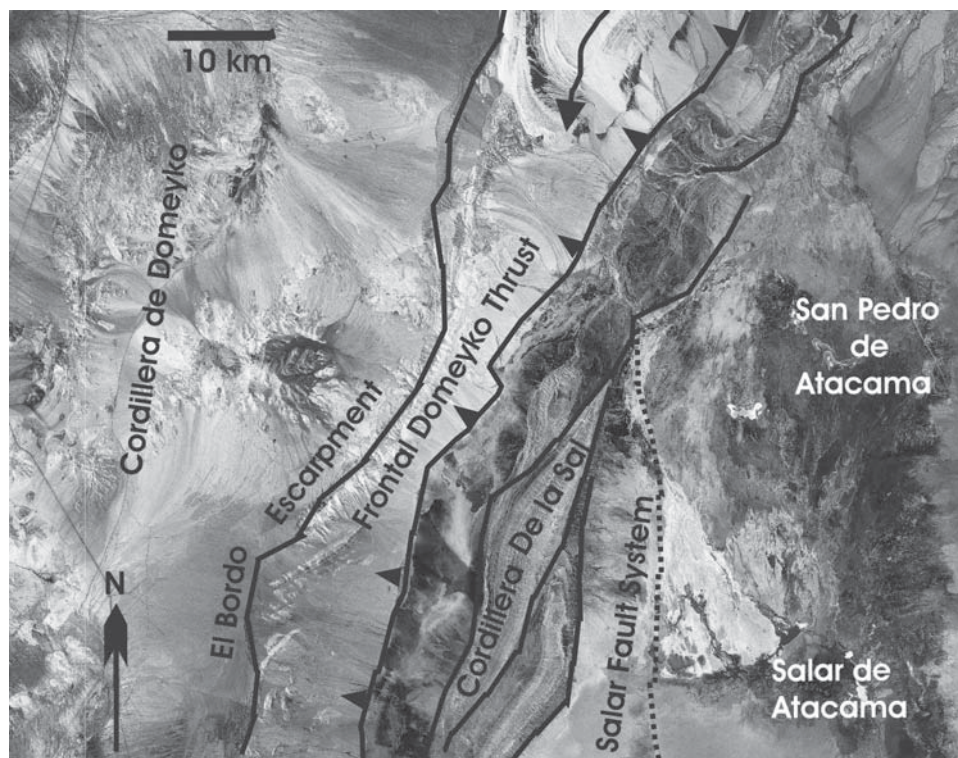


**Fig. 9.10.** Landsat TM+ (742) image of the Neogene Atacama Salar forearc basin showing the main structural features (taken from Muñoz *et al.* 2000; Flint *et al.* 1993). Critical points include the position of the Cordillera de la Sal, the El Bordo escarpment and the thrustured Domeyko Cordillera, which forms the western basin margin.

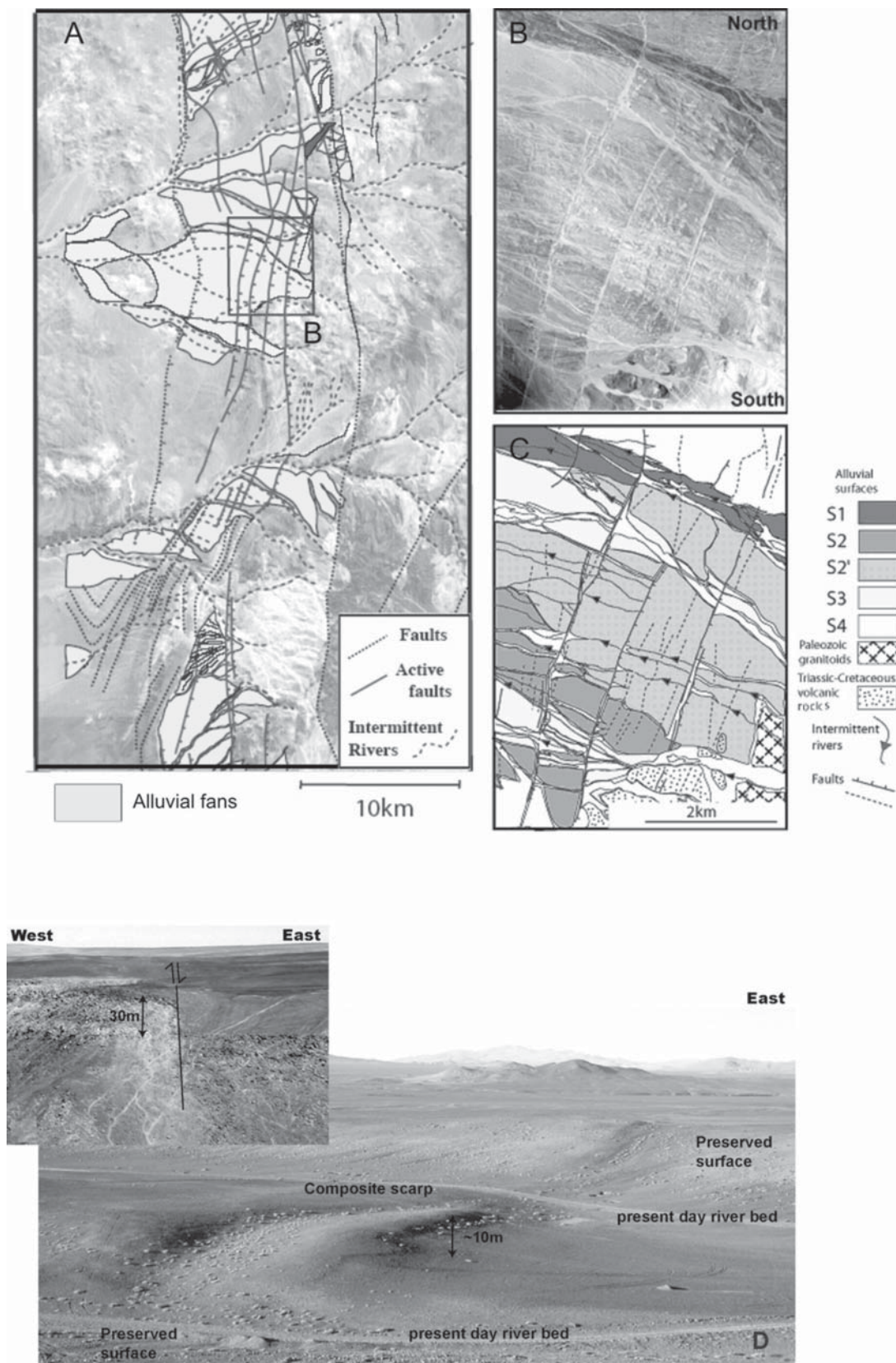


**Fig. 9.11.** (A) Morphotectonic interpretation, on Aster Satellite image, of the western flanks of Domeyko Cordillera between 25°30'S and 26°S approximately. In this area, alluvial fans are affected by vertical faults. (B) Aerial photograph and (C) interpretation of the vertical faults, in Pampa Exploradora around 3500 m. S1 to S4 are successive nested alluvial surfaces. The scarps are linear and continuous forming vertical and composite scarps about 5–10 m high, the dip direction of which (toward the east) never changes along-strike. No lateral offset can be identified along these fault traces. The scarps are coupled with neighbouring secondary synthetic faults that create small half-graben where Quaternary sediments are trapped. (D) Inset shows type example of a major normal fault scarp, with 30 m throw, cropping out in the Precordillera of the El Salvador region (view looking north to the Pampa Exploradora's flank). Main photo shows north-looking view of river-cut cross-section of a fault scarp at the Pampa Doña Ines Chica.



(Fig. 9.9B). The three most important reverse faults extend over 50 km and dip between 20° and 60° to the east. Around Belén, the contractional system is characterized by a large asymmetric anticline of 35 km wavelength, which involves thrust sheets of Precambrian–Palaeozoic basement and, to the west, sheets of syntectonic coarse-grained conglomerates and volcanic rocks. In the Chucal–Macusa area, west-vergent and east-vergent folds and faults are exposed (Riquelme 1998; Garcia 2001; Charrier *et al.* 2005b). In Chucal, an east-vergent growth anticline of 5 km wavelength has flanks dipping from 10° to 80°. Along its western border, the anticline is cut by the 40–50° east-dipping Jaropilla reverse fault, which displaces the lower Lupica Fm over the Chucal Fm. To the west, the Macusa folds are short, tight (0.5 to 2 km in wavelength) and west-vergent, forming a narrow zone of deformation. The Precambrian–Palaeozoic basement is not exposed in the Chucal–Macusa area. Three balanced cross-sections in the Western Cordillera, east of Arica, indicate a minimum post-18 Ma shortening ranging from 6 to 7 km which translates to 20% to 40%. Recent (late Holocene) tectonic activity on the border of the Western Cordillera is evidenced by shallow (<20 km) microseismic activity (Comte *et al.* 1999).

To the south, at the latitude of Pisagua, folding and faulting related to uplift have been reported to affect Miocene lavas and ignimbrites (Puchuliza, Condoriri and Utayane formations; Lahsen 1982). East of Iquique and Antofagasta, the Western Cordillera of northern Chile largely consists of Pliocene–Holocene stratovolcanoes, and Neogene tectonic features are either not exposed or have not been described. In Pica, shortening across the Precordillera and Western Cordillera has been calculated to be around 5 km (Victor *et al.* 2004). East of Copiapó, in the Claudio Gay Cordillera, Neogene east- and west-vergent deformation is represented by gentle folding and basement-involving high-angle reverse faulting (Mpodozis & Clavero 2002).

### Large-scale landscape configuration

Northern Chile can be viewed as comprising two north–south elongated neotectonic units: an inner forearc and arc domain, and an outer forearc domain. The inner forearc and arc domain comprises parts of the Central Depression, the Precordillera, the Cordillera de Domeyko and the Western Cordillera, whereas the outer forearc domain is dominated by the Coastal Cordillera.

The outer forearc domain is characterized by north–south striking normal faulting (and locally by east–west faulting), a phenomenon characteristic of, and restricted to, the Coastal Cordillera. In addition to this faulting, long-term uplift has affected the Coastal Cordillera in northern Chile, and has a major topographic expression in the prominent (up to 1000 m high) coastal cliff (Fig. 9.12). Late Pleistocene to Holocene marine terraces exposed at the foot of the Coastal Cliff register the most recent uplift pulses in the coastal area. The terraces are distributed in a staircase pattern extending from 3 to 170 m a.s.l. (Leonard & Wehmiller 1991; Niemeyer *et al.* 1996; Ortlieb *et al.* 1996). Exceptionally high elevations of late Pleistocene to Holocene marine terraces are reached on the Mejillones Peninsula where some terraces are exposed at elevations above 300–400 m a.s.l. (González *et al.* 2003). Uplift rates calculated on the basis of the age of the marine terraces and their position relative to the present-day sea level indicate values between 0.05 and 0.5 mm/year (Ortlieb *et al.* 1996; Delouis *et al.* 1998).

The deformational regimes described above indicate that the outer forearc is undergoing east–west extension orthogonal to the trench, north–south shortening and forearc uplift. These major deformation processes have been active over a time span of Miocene to late Pleistocene. Because the extensional and the contractional structures (north–south shortening) are restricted to the Coastal Cordillera, above the zone where the Nazca Plate and South American Plate are seismically coupled, it is reasonable to assume that these first-order processes are related to plate interaction. East–west directed extension has been interpreted to be a result of tectonic erosion (Niemeyer *et al.* 1996), upper plate bending (Delouis *et al.* 1998; González *et al.* 2003) and coseismic extension (Delouis *et al.* 1998; González *et al.* 2003). North–south shortening can be explained as an effect of the subduction occurring along a segment of the central Andes concave to the ocean geometry. The limited geographic distribution of reverse faults which mark the north–south shortening, which is restricted to the inner part of the central Andean oroclinal bend, strengthens this interpretation. Forearc uplift seems to be the most widely distributed tectonic process, acting over the entire length of the forearc. A number of hypotheses have been postulated to explain the long-term uplift of the forearc. The most commonly applied explanation is the underplating of crustal material beneath the Coastal Cordillera, along the seismically coupled zone (Armijo & Thiele 1990; Delouis *et al.* 1998). In this context, uplift would be the result of a deep-seated process of crustal thickening. An alternative

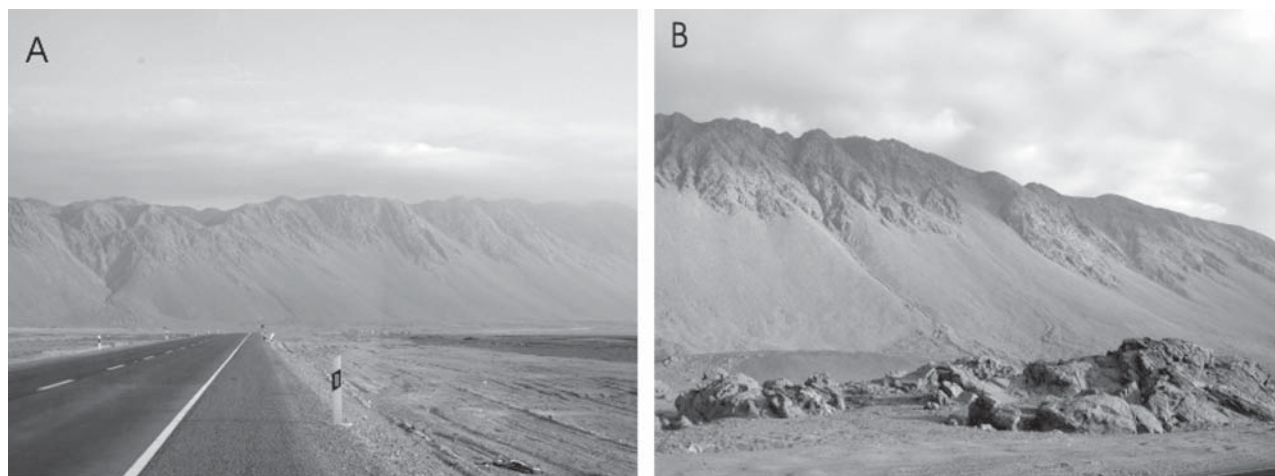


**Fig. 9.12.** (A) Panoramic view and (B) detail of coastal cliff exposed close to the Loa River. The coastal cliff crest is formed by Mesozoic plutonic rocks. Note the detritus talus formed mainly by diffusion. The coastal cliff crest has an angle of 56° and the detritus talus has a stable angle of 30°. View looking to the SE.

process is the progressive indentation of the Nazca Plate beneath the South American plate. Because east–west extension and forearc uplift are regionally the most widely distributed type of tectonic activity, it is reasonable to infer that they represent the direct morphological expression of plate convergence in the outer forearc.

The inner forearc and arc domain of northern Chile is characterized by double-vergent folding and thrusting that can be related to overall east–west shortening and uplift affecting the high central Andes. In the Altiplano segment, the Precordillera was mainly uplifted by west-vergent folding in connection with reactivation of high-angle reverse faults with large vertical throws (García 2001; Victor *et al.* 2004; Pinto *et al.* 2004b; Farias *et al.* 2005b). The recorded vertical throws along these reverse faults can alone explain the differences in elevation between the Precordillera and Central Depression. The Western Cordillera is configured by west-vergent moderate-angle reverse faults involving larger shortening than in the Precordillera, and it forms part of the fold and thrust belt that affect the backarc. However, two questions concerning the role that the folding and faulting play on the Neogene uplift of the Altiplano can be raised: (1) What was the elevation of the Altiplano at the beginning of the Neogene? (2) Does the mentioned shortening explain the Neogene uplift of the Western Cordillera?

In relation to the first question, sedimentological evidence from the Bolivian Altiplano and Central Depression indicates that the Western Cordillera and Precordillera were uplifted areas of high relief subject to erosion during the Oligocene (Lamb *et al.* 1997; Horton *et al.* 2001; García 2001). Towards the south, between the latitudes of Antofagasta and El Salado, fission track data indicate that an important episode of exhumation occurred in the Domeyko Cordillera in Eocene–early Oligocene time (Maksaev & Zentilli 1999). Riquelme *et al.* (2003) documented this exhumation process from field data and argued that the Precordillera was already at least 2500–3000 m above sea level at that time. Thus, most of the present-day altitude of the inner forearc and arc region was probably reached prior to Neogene times.

In relation to the second question, various authors argue that the main uplift episode of the Altiplano–Puna occurred during the Neogene (e.g. Isacks 1988; Baby *et al.* 1997; Gregory-Wodzicki 2000). However, assuming an important pre-Neogene altitude in the Western Cordillera, Neogene shortening by itself cannot explain the present-day elevation of the Altiplano. In order to reach its present-day altitude, geophysical and petrological studies consider additional processes have contributed to crustal thickening (e.g. Giese *et al.* 1999). Additional crustal thickening from magmatic addition (e.g. Gill 1981; Hoke *et al.* 1994; Kono *et al.* 1989; Francis & Hawkesworth 1994), lithospheric thinning and removal of the subcrustal lithosphere (Isacks 1988; Whitman *et al.* 1996; Lamb *et al.* 1997; Beck & Zandt 2002), underplating of material removed from the forearc by subduction erosion (e.g. Schmitz 1994; Baby *et al.* 1997; Hartley *et al.* 2000), or ductile mass transfers within the lower crust (Kley *et al.* 1999; Beck & Zandt 2002; Gerbault *et al.* 2002; Husson & Sempere 2003) have been proposed.

The effects of crustal thickening and uplift in the inner forearc domain have been to produce a westward regional tilting and/or crustal flexuring (e.g. Isacks 1988; Lamb *et al.* 1997). At the latitude of Copiapó–El Salvador, deep vertical incision in the forearc region can only be explained by post-10 Ma tilting of the inner forearc and arc domain (Riquelme *et al.* 2003). Neogene shortening without significant strike-slip motions is recorded in the Domeyko Cordillera. Field evidence shows that this latest deformation episode corresponds to minor reactivation of pre-existing structures since late Miocene times (e.g. Jordan *et al.* 2002; Audin *et al.* 2003; Soto *et al.* 2005). Fault reactivation can occur under stress levels lower

than those needed for creating new faults (Handin 1969). Moreover, if a previous fault pattern is present, fault reactivation rather than formation of new faults is frequently observed, even if the consecutive deformation episodes are not coaxial, in particular if the latest deformation episodes are smaller (e.g. Brun & Nalpas 1996; Dubois *et al.* 2002). Thus, it is probable that the latest tectonic activity observed in the Precordillera and Cordillera de Domeyko corresponds to low-intensity episodes of deformation that reactivated Eocene–Oligocene structures originally related to uplift of the western Andean margin within a compressive regime.

Convergence controlling the shortening of the forearc is expressed by thrusting of western border Precordillera over the Central Depression. In contrast, forearc uplift localized on the Coastal Cordillera is a deep-seated process and not directly connected with near-surface faulting. Given this background, the popular idea that the Atacama Fault System controls the uplift of the Coastal Cordillera has to be reconsidered. East–west extension and north–south shortening control only the second-order morphostructural features of the forearc by faulting and differential uplift.

To summarize, two longitudinal structural domains can be proposed for the Neogene in the forearc region: an outer forearc domain comprising the Coastal Cordillera, and an inner forearc and magmatic arc domain comprising the western part of the Central Depression, Precordillera, Domeyko Cordillera and Western Cordillera. The outer forearc exhibits north–south striking normal faults consistent with east–west directed extension, as well as forearc uplift evidenced by the landscape features (coastal cliff >1000 m high, Late Pleistocene–Holocene marine terraces). Both east–west extension and forearc uplift result from the interaction of the seismically coupled Nazca and South America plates. East–west extension may be attributed to a number of processes: tectonic erosion, upper plate bending or coseismic extension. Forearc uplift results from underplating of crustal material beneath the Coastal Cordillera or from progressive indentation of the Nazca Plate beneath South America. Trench-parallel shortening is restricted and localized to where the plate boundary has a concave-towards-sea geometry (i.e. the oroclinal bend of the central Andes). The inner forearc and magmatic arc domain is characterized by high-angle reverse faulting and folding (Altiplano segment) and minor reactivation of older structures (Puna segment). This most recent tectonic activity in the inner forearc region is related to the uplift of the western Andean margin within a compressive regime. Uplift localized in the outer forearc in the Coastal Cordillera is a deep-seated process, while shortening controlled by convergence is expressed by thrusting and folding in the inner forearc region.

### **Pliocene–Pleistocene state of stress for the central and southern Chilean Andes (A.L. & J.C.)**

This section summarizes the nature and significance of Plio-Pleistocene deformation of the central and southern Chilean Andes between 33°S and 46°S (Fig. 9.13). In contrast with northern Chile, where extremely arid conditions allow the superb preservation of fault scarps and other structural features associated with Neogene to Recent deformation, the more humid climate and concomitant higher erosion rates of central and southern Chile make direct observation of many morphotectonic structures difficult. One way to overcome this limitation was to map a number of well-exposed structural sites located close to or on large-scale lineaments believed to represent major fault zones located at the boundaries between the main morphological units of the Andes. The outcrop-scale mapping of these structural sites consisted in identifying main rock units and the nature, kinematics and relative age of



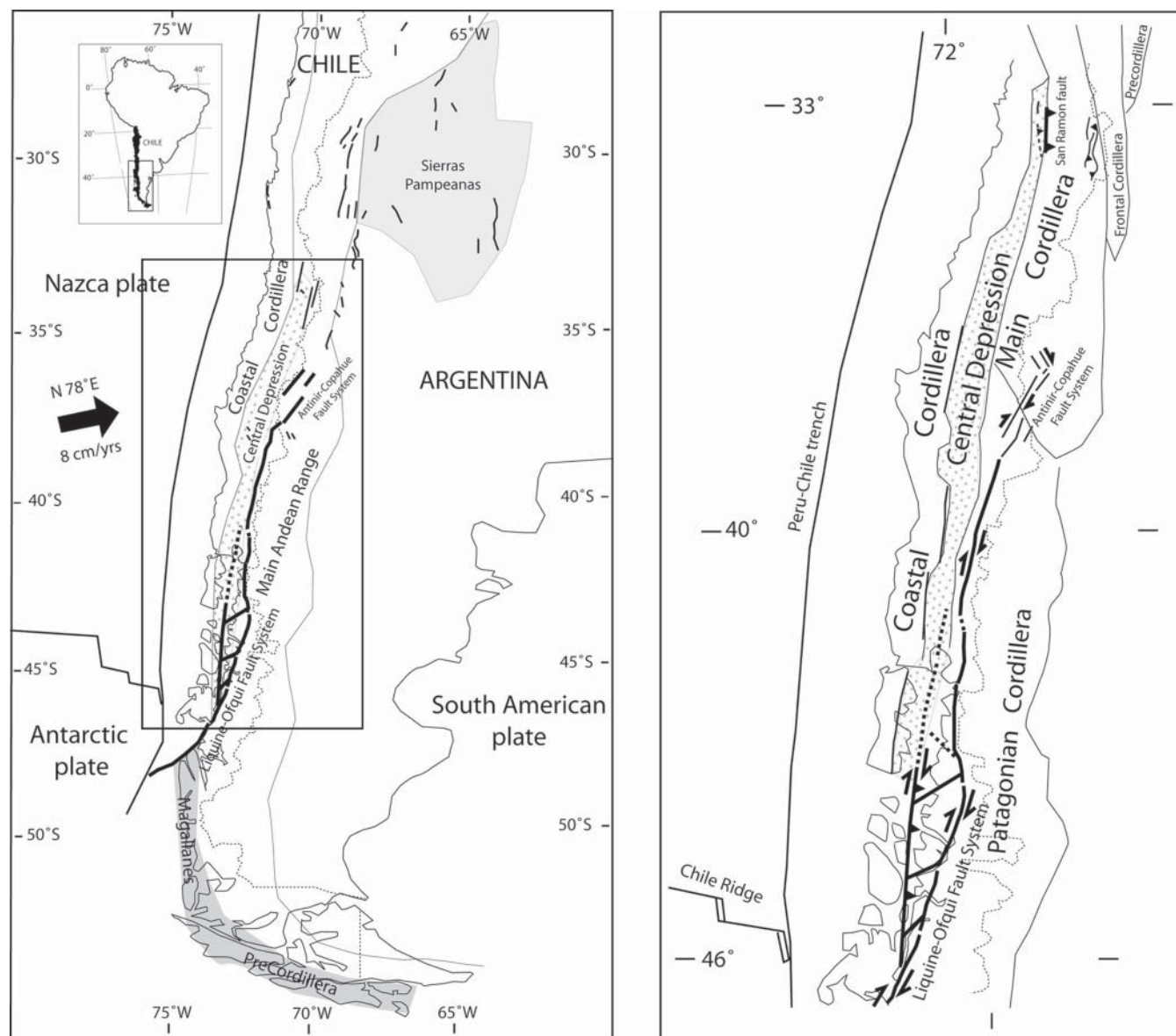


**Fig. 9.13.** Regional schematic map showing the main morphological units of the Andes for central and southern Chile. Neogene regional fault systems are also indicated.

mesoscopic faults and folds. Fault-slip data from each site were then used to calculate one or more stress tensors, believed to represent different tectonic events. Different authors have treated fault-slip data for the Andes as yielding local stress (e.g. Lavenu & Cembrano 1999b) or strain tensors (e.g. González *et al.* 2003; Allmendinger *et al.* 2005). Whether it is more convenient or accurate to obtain stress or strain from field data is the subject of a long-standing discussion that is beyond the scope of this review (e.g. Bott 1959; Carey & Brunier 1974; Marrett & Allmendinger 1990). However, for internal consistency we will assume that the principal directions of stress are more or less coaxial with those of incremental strain for regions that have not undergone significant block rotations, an assumption that can be considered fair for large-scale deformation studies such as the one addressed here.

In this part of the chapter we provide an integrative account of the most geologically significant structural sites of the central and southern Chilean Andes for which a Pliocene and/or Pleistocene stress or strain tensor has been calculated from fault-slip

data. We have selected those sites for which good structural data can be placed into a regional context based on a good constraint of both kinematics and age. For the sake of clarity on data presentation and discussion, we have divided the central (33–39°S) and southern (39–46°S) Chilean Andes into margin-parallel, morphostructural domains that exhibit internally consistent geology and kinematics.

Although some authors have restricted the term ‘neotectonics’ to the last recorded deformation event of an area, we deliberately include Pliocene to Recent deformations to better understand the nature of the link between temporal and spatial changes in plate boundary conditions (rates, subduction angle, degree of coupling) and tectonics of the upper plate.

#### **Geological and morphotectonic framework**

The Andes of central and southern Chile consist of three tectonically distinct parallel domains: (i) a forearc zone located between the Peru–Chile Trench and the Main Cordillera, in which the Coastal Cordillera and Central Depression are

located; (ii) a magmatic arc in the Main Cordillera, which is the active volcanic zone; and (iii) a foreland zone in Argentina where the most recent deformations are documented (e.g. Costa *et al.* 2000b,c; Diraison *et al.* 1998; Folguera *et al.* 2004) (Fig. 9.13).

#### *Coastal Cordillera*

The Coastal Cordillera between 33°S and 46°S is a discontinuous morphological feature made up of Mesozoic volcano-sedimentary rocks intruded by coeval plutonic belts. Late Palaeozoic to Jurassic granitoids and metamorphic rocks occur along the coast between 36°S and 46°S, west of the Coastal Cordillera, and represent the basement upon which the Andes have been built (Hervé 1987a, b). A few patches of Cenozoic sedimentary units occur west of the Coastal Cordillera proper along the coast at Navidad (33°S) and Península de Arauco (37°S).

The Coastal Cordillera varies in altitude from up to 2 km at 33°S to *c.* 0.5 km at 46°S. Available geological and fission track data suggest that the Coastal Cordillera of central Chile underwent a period of rapid exhumation at *c.* 100 Ma, at the end of a major compressional/transpressional event (e.g. Cembrano *et al.* 2003; Arancibia 2004; Parada *et al.* 2005b). Evidence for neotectonic deformation along the Coastal Cordillera of central and southern Chile is scarce and of poorly known age (e.g. Lavenu & Cembrano 1999b). However, a few sites show good evidence of Pliocene and Pleistocene deformation; these will be described below.

#### *Central Valley*

The Central Valley (sometimes also referred to as the Central Depression) is a north–south trending morphostructural domain running between the Coastal Cordillera and the Main Cordillera between 33°S (close to Santiago) and 46°S (Ofqui Isthmus). The valley is filled with 1500 to 5000 m of Oligocene to Recent continental and sometimes marine (?) deposits (Elgueta *et al.* 2000a), and whilst never more than 75 km wide, it concentrates most of Chile's population. The western and eastern boundaries of the Central Valley have long been thought to be normal faults defining a graben structure (Aubouin *et al.* 1973a; Laugenie 1982; Cisternas & Frutos 1994). However, more recent work (e.g. Lavenu & Cembrano 1999b; Farias *et al.* 2005b; Fock *et al.* 2005) has shown that these boundaries are locally represented by eroded fault scarps with complex kinematics. The eastern limit of the Central Valley from 33°S to 46°S is currently regarded as an eroded fault system made up of Miocene to Pliocene strike-slip and west-verging reverse faults (e.g. Fock *et al.* 2005; Cembrano *et al.* 2002). The boundary between the Central Valley and the Main Cordillera from 39°S to 46°S, corresponds well with the western branch of the Liquiñe–Ofqui Fault Zone (LOFZ), marked by a straight NNE-trending lineament. Limited field evidence along this lineament shows a complex system of Pliocene (*c.* 4 Ma) dextral strike-slip and reverse ductile to brittle fault zones developed on the west flank of the Patagonian Batholith Miocene belt (e.g. Lavenu & Cembrano 1999b; Cembrano *et al.* 2000, 2002). The LOFZ, which controls the morphology of channels and fiords, places deep structural levels of the Main Cordillera represented by the Patagonian Batholith, on top of upper structural levels of the Central Valley documented here by mid-Tertiary volcanic and sedimentary rocks (Lavenu & Cembrano 1999b; Pankhurst *et al.* 1999; Cembrano *et al.* 2002; Thomson 2002).

#### *Main Cordillera*

The Main Cordillera between 33°S and 39°S is characterized by folded and faulted Meso-Cenozoic volcanosedimentary units intruded by Late Miocene to Pliocene plutonic rocks and the present-day volcanic arc. Altitudes vary between *c.* 6000 m in the north down to 3000 m in the south, with an average width of 80 to 100 km. The most important regional-scale structures at these latitudes are a series of east-verging Neogene fold and

thrust belts that developed within and to the east of the Main Cordillera in the frontal Cordillera and foreland of Argentina (Ramos 1988a; Charrier *et al.* 2002; Giambiagi *et al.* 2003). Neogene deformation on the Chilean side of the Cordillera is more limited. However, recent work by Farias *et al.* (2005b) suggests that the western part of the Main Cordillera east of Santiago has been differentially uplifted during the Neogene by a west-verging fault system that may still be active (San Ramon fault, see Fig. 9.13).

Neotectonic deformation along and east of the Main Range between 37°S and 39°S is well-represented by the Antiñir–Copahue Fault System in Argentina and by the northern termination of the Liquiñe–Ofqui Fault System in Chile (e.g. Folguera *et al.* 2004). The Antiñir–Copahue system (Fig. 9.13) is formed by an east-verging fan of high-angle transpressional and transtensional faults affecting Pliocene to Pleistocene volcanic rocks. Some recent deformation of unconsolidated deposits has also been reported (Folguera *et al.* 2004), which emphasizes the importance of these faults as active Andean structures. The Antiñir–Copahue system of Argentina gives way southward to the Liquiñe–Ofqui Fault Zone. This fault system is at these latitudes represented by a dextral transtensional array of master NNE-striking right-lateral faults and a subsidiary set of NE- and ENE-striking oblique-slip and normal faults. Both strike-slip and normal faults are spatially and temporally associated with stratovolcanoes and caldera structures such as the El Agrio Caldera (Melnick *et al.* 2002; Folguera *et al.* 2004, 2005).

The most important Neogene regional structure of the Main Cordillera between 39°S and 46°S latitude is the *c.* 1000-km-long Liquiñe–Ofqui Fault Zone (Hervé 1976; Hervé *et al.* 1979a), which consists of two overstepping NNE-striking master faults joined by a series of en echelon NE-striking subsidiary faults forming a strike-slip duplex structure (Fig. 9.13). Field observations combined with Ar/Ar and fission track thermochronology along the LOFZ document a main event of dextral transpressional ductile deformation at *c.* 4 Ma, followed by brittle compressional to strike-slip deformation after 3.8 Ma and 1.6 Ma, respectively (Hervé 1994; Cembrano *et al.* 1996, 2000, 2002; Lavenu & Cembrano 1999b; Thomson 2002).

#### *Pliocene state of stress between 33°S and 46°S*

Previous work shows that the state of stress in the Andes during latest Pliocene time (1.8–3 Ma) had two main characteristics: it was compressive, and it had an approximate east–west maximum horizontal stress direction throughout the whole Andean chain. This deformation is well documented from Ecuador to southern Chile and from the Pacific coast to the Subandean zone in Peru, Bolivia, and foreland regions in Argentina (Lavenu *et al.* 1989, 1995; Allmendinger *et al.* 1989; Lavenu & Mercier 1991; Mercier *et al.* 1992; Urreiztieta *et al.* 1996; Niemeyer *et al.* 1996; Diraison *et al.* 1998; Lavenu & Cembrano 1999b; Gonzalez *et al.* 2003). A summary overview of Pliocene deformation for the central and southern Andes is provided by Figure 9.14 which shows the compression direction resulting from fault-slip data inversion for the sites described in this study plus others selected from the literature (e.g. Martinez 1980; Jordan *et al.* 1983b; Lavenu & Mercier 1991).

#### *Northern segment between 33°S and 39°S: Coastal Cordillera*

**Navidad (34°S).** The Miocene Navidad basin, west of the Coastal Cordillera of central Chile exhibits evidence of several deformation events of Miocene to Pliocene age (Lavenu & Encinas 2005). After a widespread extensional Miocene to Pliocene episode, the basin underwent an important uplift event followed by NW–SE directed extension. During the late Pliocene, a compressive regime ( $\sigma_1 = N250^\circ E$ ) deformed the basin deposits as indicated by mostly north–south striking reverse faults. The last deformation episode is represented by north–south striking normal faults compatible with east–west extension of the outer forearc (Fig. 9.15).



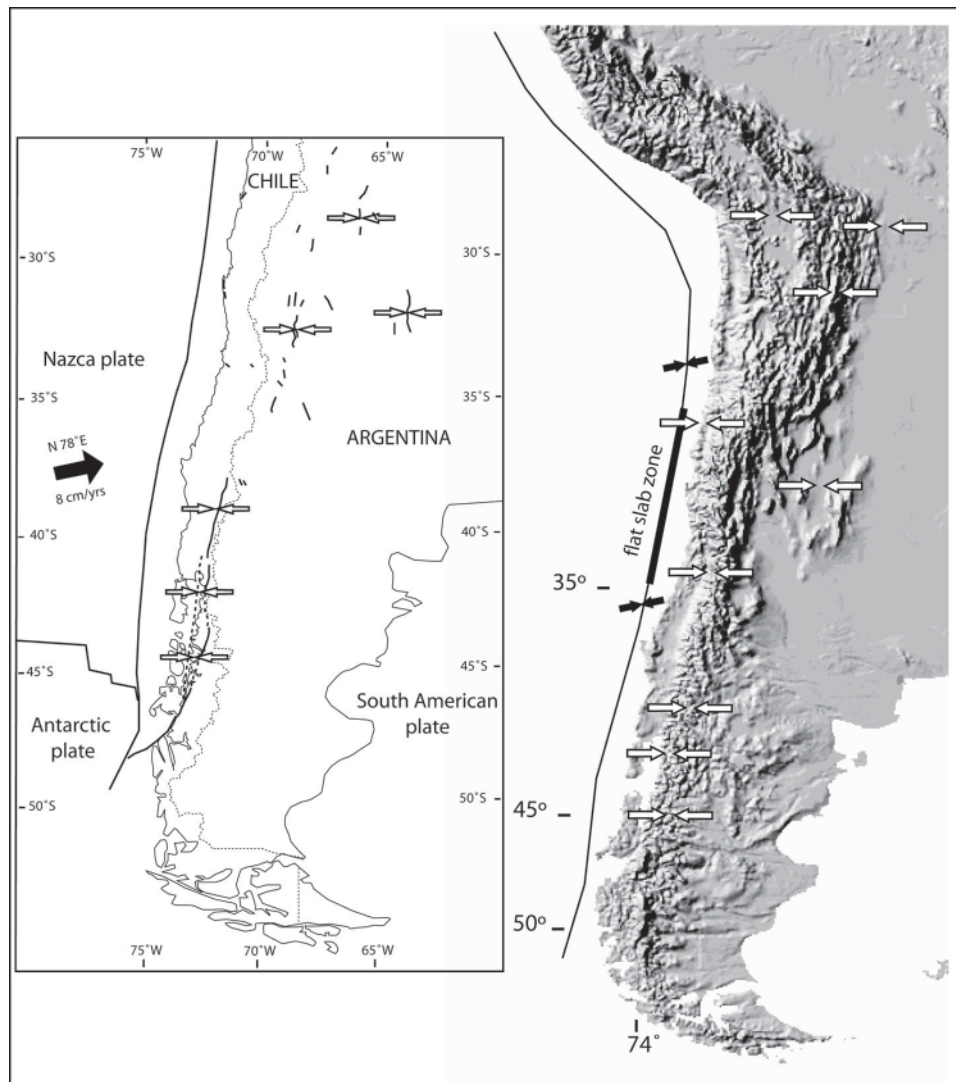


**Fig. 9.14.** Summary figure showing the results of the microtectonic analysis of Pliocene faults from central and southern Chile and other parts of the Andes, for comparison. The compressional east–west tectonic regime documented in Chile has also been recorded in the Altiplano, Eastern Cordillera, and well into the foreland (e.g. Martinez 1980; Jordan *et al.* 1983b; Lavenu & Mercier 1991).

**Península de Arauco (38°S).** Dense forest and limited access to the area prevent systematic structural studies of the Arauco Peninsula, although two broad morphostructural domains can be identified. The first of these is an eastern domain consisting of a Palaeozoic metamorphic basement and a Triassic–Cretaceous sedimentary cover. The second is a western domain (Arauco Peninsula) which forms a low-altitude zone marked by marine terraces close to the coast: an upper terrace between 180 and 200 m, two intermediate ones at 75–100 m and 50 m, and a lowermost one at 25 m. This coastal block consists of Eocene deposits and a Mio-Pliocene basin, with the latter forming a graben flanked to the west and east by NNE-striking normal faults (Martinez-Pardo & Osorio 1968; Ferraris & Bonilla 1981; Martinez-Pardo 1990).

*Northern segment between 33°S and 39°S: Central Valley*

At 36°S, the boundary between the Central Valley and the Main Range is marked by regional faults striking N30°E. These faults cut Oligocene–Miocene volcanic rocks, which document a vertical displacement (west-side-down) of *c.* 1000 m. Mesoscopic faults exposed along the eroded fault scarp on these volcanic rocks are mainly strike-slip, compatible with either east–west or north–south compression. The western flank of the Central

Valley is characterized by a system of north–south to N10°E master faults and N30–40°E subsidiary faults. Mesozoic and Neogene rocks exhibit mesoscopic strike-slip and reverse faults with minor evidence for normal faults. The latter have been interpreted as gravitational structures associated with topography.

*Northern segment between 33°S and 39°S: Main Cordillera*

**Los Andes, Farellones, Mina El Teniente (33–34°S).** A systematic study of the Neotectonic deformation along the Main Range was undertaken in the San Felipe–Los Andes region, at the town of Farellones east of Santiago and at El Teniente copper deposit, covering a region of central Chile between 33°S and 35°S. A 4.5 Ma breccia pipe (Cuadra 1986), the Braden Breccia, cuts through the core of El Teniente copper deposit and provides an excellent opportunity to map Pliocene–Pleistocene(?) deformations. Kinematic analysis of fault-slip data from the Braden Breccia document two independent and superposed compressional events. An older event, characterized by a N60°E-trending  $\sigma_1$ , and a younger event with a north–south trending  $\sigma_1$ . Additional fault-slip data coming from a nearby younger 2.8 Ma lamprophyric dyke (Cuadra 1986), record only the later north–south compressional event, confirming a likely

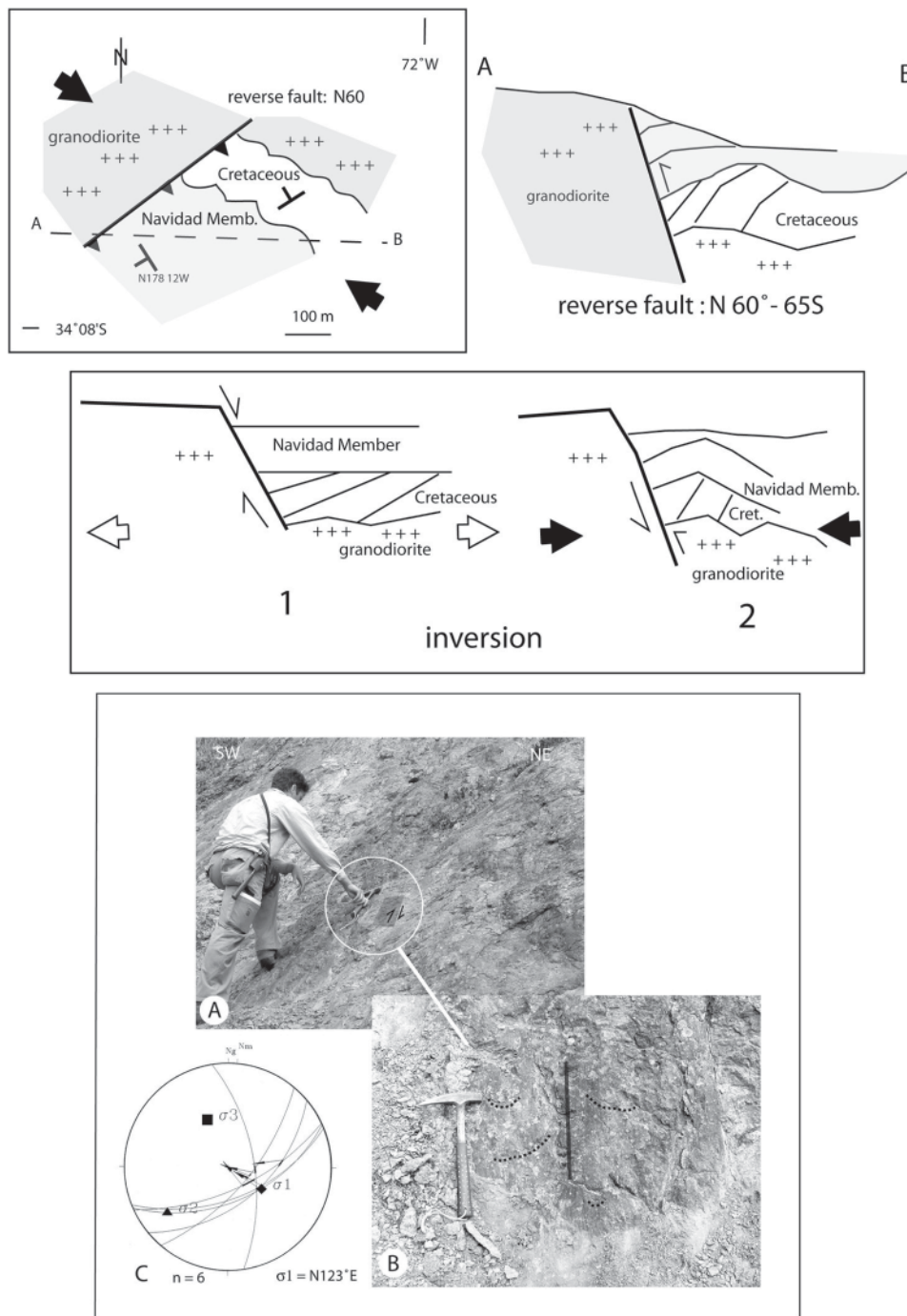


**Fig. 9.15.** Field evidence for ESE–WNW compressional deformation in the Neogene Navidad basin of central Chile. A reverse fault places Cretaceous to Neogene strata on top of a Palaeozoic granodiorite. This fault is interpreted as an early normal Neogene fault reactivated as a reverse fault during compression. Reverse reactivation is supported by overprinting kinematic indicators on the fault surface (Lavenu & Encinas 2005).

Pleistocene age for this younger compression that will be accounted for later in the text (Fig. 9.16).

*Southern segment between 39°S and 46°S: Coastal Cordillera Taitao Peninsula (46°S).* Only a few studies of brittle deformation have addressed the Neogene tectonics of the southernmost part of the Coastal Cordillera; available data only describe the geometry of faulting at the regional scale close to the Nazca–South America–Antarctica triple-junction (e.g. Forsythe & Nelson 1985; Forsythe *et al.* 1986). According to Veloso (2001),

a Pliocene compression–transpression event, with  $\sigma_1$  close to N260°E, is documented in the Taitao Ophiolite (dated 11–6 Ma) and the Seno Hoppner pluton (dated 6.2–5.5 Ma)

*Southern segment between 39°S and 46°S: Main Cordillera Reloncavi (41°S).* On both sides of Estuario Reloncavi, centimetre- to decametre-scale striated fault planes cut all the plutonic units ranging in age from Cretaceous to Miocene, whereas Quaternary sedimentary and volcanic rocks do not show any evidence of faulting. Most faults are steeply dipping



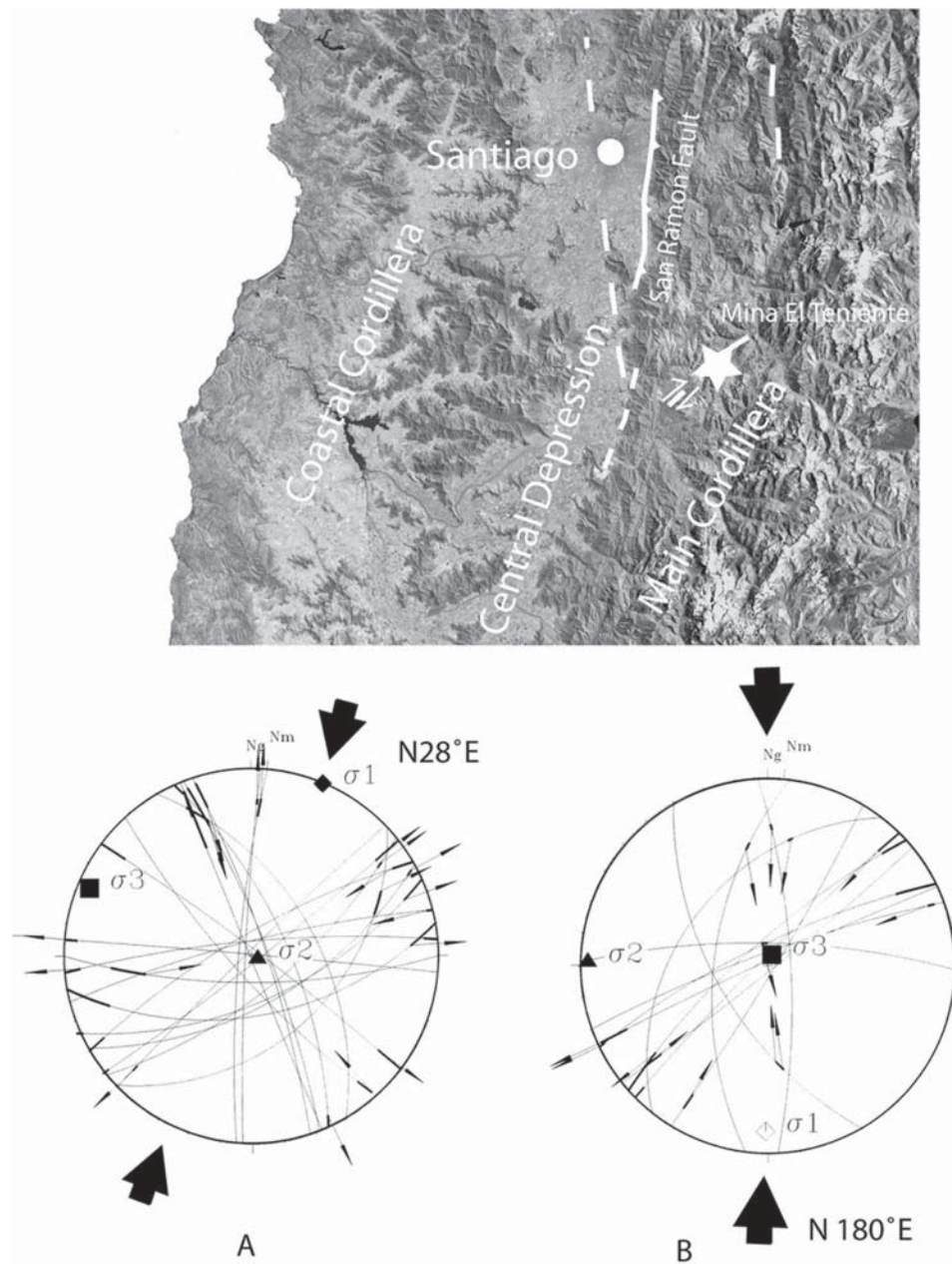


Fig. 9.16. Regional map showing the location of structural sites in the Main Cordillera of Central Chile for which fault-slip data were obtained.

(>60°), with striae ranging in pitch from subhorizontal to subvertical. Two distinct homogeneous populations of faults were identified in the Reloncaví region. The first is represented in Figure 9.17, which includes faults with a predominant strike-slip component, and a few with predominant dip-slip component. Faults with strike ranging between N337°E and N065°E (average N020°E) show right-lateral slip sense; faults striking between N084°E and N115°E (average around N100°E) are left-lateral; and faults striking WNW are reverse-slip. The kinematic analysis of these mesoscopic faults is consistent with a compressional *c.* east–west trending stress regime suggested by the first fault population:  $\sigma_1 = 261^\circ, 05^\circ$ ;  $\sigma_2 = 171^\circ, 07^\circ$ ;  $\sigma_3 = 28^\circ, 82^\circ$ . A second diagram (Fig. 9.17) shows the second homogeneous population of faults identified; most have a significant down-dip component, although some strike-slip faults are also included. These younger faults will be further described in the Pleistocene deformation section.

**Puyuhuapi, Queulat, Puerto Cisnes (44°S).** Four sites were measured in intrusive rocks with late Miocene to Pliocene Ar/Ar dates (5.5 and 10 Ma (Hervé *et al.* 1993) and 5.3 and 13.3 Ma (Cembrano 1998)) and two were measured in Patagonian batholithic rocks of uncertain age. The main direction of compression in this case is also close to east–west, the directions of  $\sigma_1$  being between ENE–WSW (N237°, 8°) and WNW–ESE (N101°, 8°). In most cases, the tectonic regime is found to be compressional; in some cases it is a strike-slip compressional regime (Fig. 9.18). Another, younger fault population has been identified at some of these sites and will be described in the next section on Pleistocene deformation.

#### *Pleistocene state of stress between 33°S and 46°S*

In contrast with the generalized Pliocene compression throughout most of the Chilean Andes between 33°S and 46°S, fault-slip analysis on several sites from the coast to the main range



E W

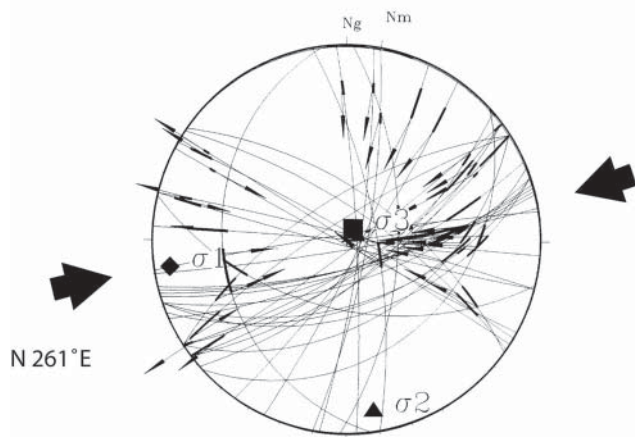


**Fig. 9.17.** The Liquiñe–Ofqui Fault System in Reloncavi represented by subvertical faults on Miocene plutons. Dextral kinematic indicators are observed on NNE-striking faults. Fault-slip analysis yields a compressional Pliocene stress tensor, in which  $\sigma_1$  strikes N261°E.

suggests that during Pleistocene time, rather than one generalized tectonic episode, there were several main deformational events of different nature and spatial distribution.

#### *Northern segment between 33°S and 39°S Coastal Cordillera*

Two types of Pleistocene deformations are recognized along the Chilean forearc. The first is east–west extensional deformation that affects large portions of the outer forearc of northern Chile including the Mejillones Peninsula and the northern Atacama Fault Zone (23°S), the Caldera coast area (27–28°S), the Altos de Talinay Peninsula (30–31°S) near La Serena, and the Arauco Peninsula (37–38°S) (e.g. Marquardt 1999; Benado 2000; González *et al.* 2003; Marquardt *et al.* 2004). All these sites lie along the coastline at a distance of 70–90 km from the offshore trench. West- or more frequently east-dipping normal faults cut uplifted Quaternary marine terraces and their deposits. On the Caldera coast and Mejillones Peninsula, the extensional deformation is younger than 400 ka. The second type of deformation is a north–south shortening in the Coastal Cordillera, the Central Valley and the Main Cordillera, west of the volcanic arc.

**San Antonio (34°S).** Close to the coast, in the Coastal Cordillera along the road between Melipilla and San Antonio, Neogene to Pleistocene marine sediments of the Navidad Formation and Potrero Alto strata (Valenzuela 1992; Wall

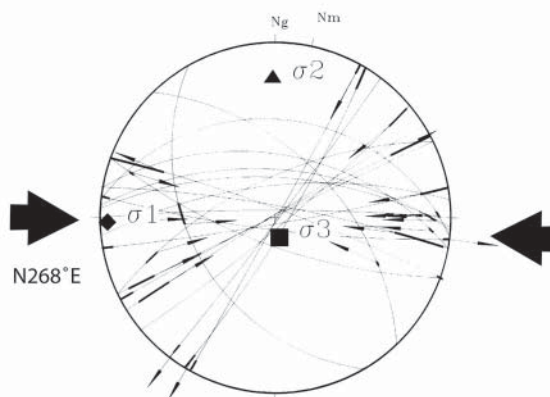
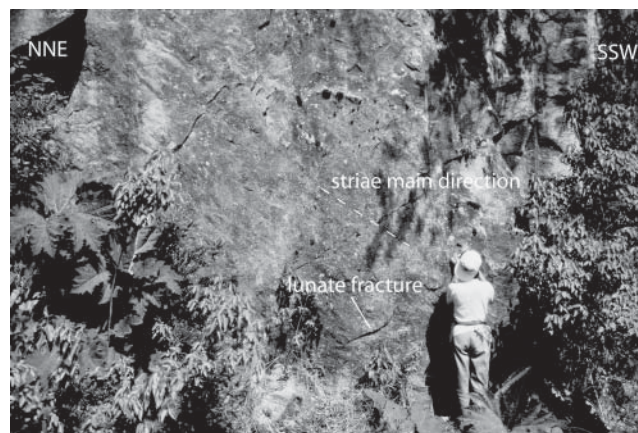


**Fig. 9.18.** The Liquiñe–Ofqui Fault System in Puyuhuapi is also represented by vertical dextral strike-slip fault planes cutting Miocene plutons. A compressional Neogene stress tensor is characterized by a subhorizontal  $\sigma_1$  striking N268°E.

*et al.* 1996) are cut by a subhorizontal erosion surface. This surface forms a pediment of late Pliocene to early Pleistocene age. A Palaeozoic granitic gneiss has been emplaced over Pleistocene sandy sediments of the Potrero Alto strata along *c.* east–west striking reverse faults. Mesoscopic (decimetric to metric) faults with centimetre- to metre-scale displacements affecting both the Palaeozoic gneisses and the Pleistocene strata show well-defined striae. Fault-slip data from this site are compatible with a N185°E-trending, horizontal  $\sigma_1$ , and a vertical  $\sigma_3$  (Lavenue & Cembrano 1999b) (Fig. 9.19).

**Península de Arauco.** East of the peninsula, between Curanilahue and Ramadillas, there is an eroded fault scarp. This scarp locally exhibits north–south striking normal faults that place Neogene–Pleistocene (?) marine sediments against the Palaeozoic–Mesozoic basement. Fault-slip data from these localities were insufficient to obtain a local stress tensor; however, all normal faults are compatible with roughly east–west trending extension of uncertain age.

#### *Northern segment between 33°S and 39°S: Central Valley*

**Esperanza (38°S).** Pleistocene terrace sediments filling the Central Valley at Esperanza are cut by reverse faults showing metre-scale displacements. Striae on these faults are compatible with a subhorizontal  $\sigma_1$  = N359°E and  $\sigma_2$  = N90°E (Lavenue & Cembrano 1999b). A similar geometry and kinematics can be found farther south in the Central Valley at Victoria, where Pleistocene fluvial sediments of the Quilleco polygenetic cone (Thiele *et al.* 1998) are cut and displaced by a reverse fault striking N150°E. This fault lies along a lineament cutting across



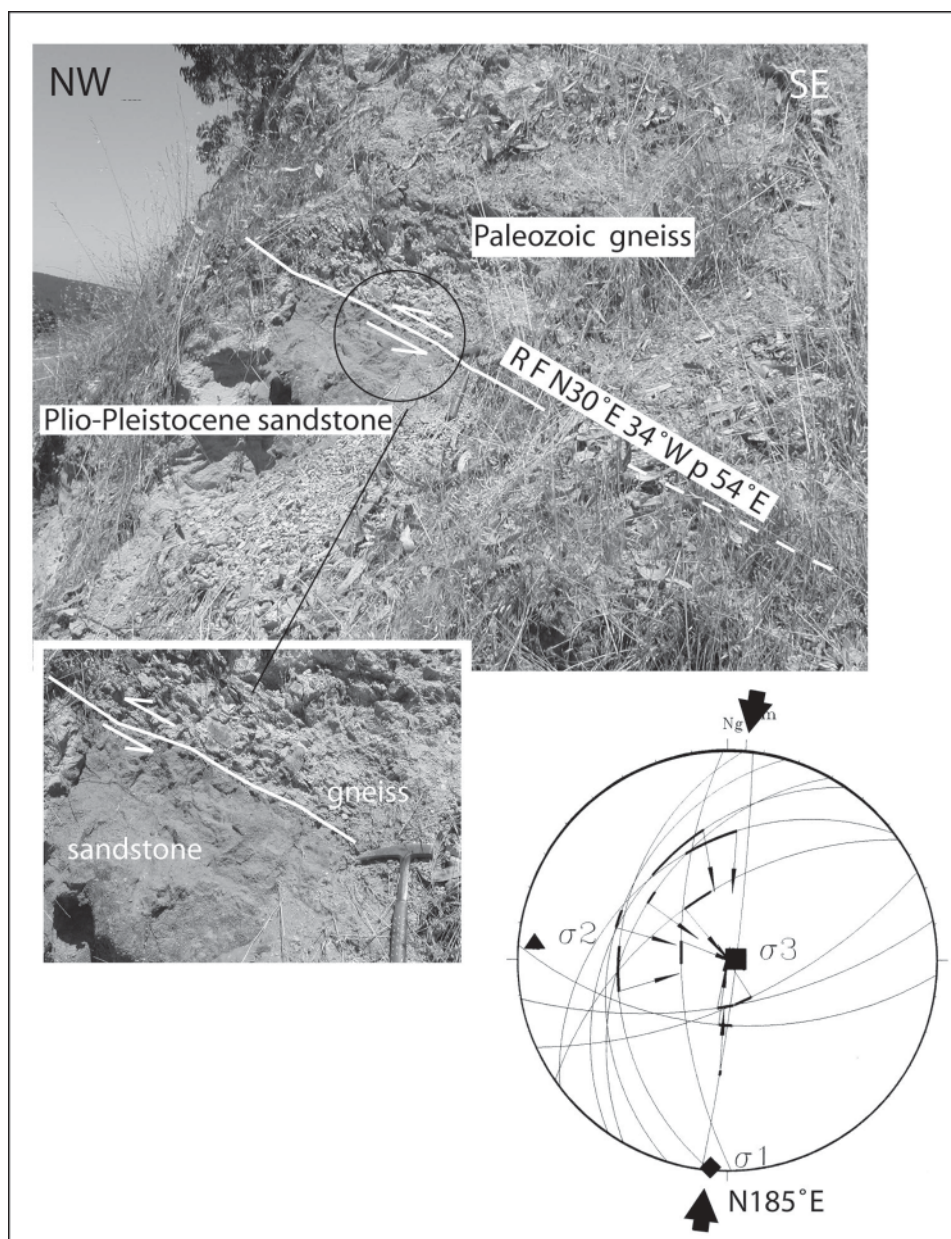


**Fig. 9.19.** Field evidence for Pleistocene, north-south trending compression in the forearc of Central Chile, near San Antonio. Mesoscopic faults with centrimetre- to metre-scale reverse sense of displacement affect both the Palaeozoic gneisses and the Pleistocene strata showing well-defined striae.  $\sigma_1$ , as obtained from fault slip data, trends N185°E.

the Palaeozoic basement. Fault-slip analysis documents a north-south to NNE compressional axis (Fig. 9.20).

**Victoria (38°S).** Pleistocene sediments of the Quilleco polygenetic cone (Thiele *et al.* 1998) exposed on the bank of the Río Traiguén are affected by a N150°E-striking reverse fault with a metre-scale vertical throw. This fault also lies along a lineament cutting across the Palaeozoic basement suggesting local Quaternary reactivation. A limited number of faults and striae are compatible with a north-south to NNE compressional axis similar to that calculated from Esperanza (Fig. 9.20).

*Northern segment between 33°S and 39°S: Main Cordillera*

**Cajón del Maipo (34°S).** Five levels of fluvial terraces occur along the left margin of the Maipo river SE of Santiago. These terraces lie on top of a late Oligocene-early Miocene basement belonging to the Abanico and Farellones formations of central Chile (Elgueta *et al.* 2000a). Close to the Colorado river

confluence with the Maipo river, these terraces, located between 880 and 1050 m above sea level, are well exposed in a gravel quarry. The highest (i.e. oldest) terrace is formed by conglomerates and sandstones with intercalated, probably reworked, ash layers. These can be considered as part of a 0.45 Ma ignimbrite deposit which is widely distributed throughout the Maipo Valley and Central Valley close to Santiago (Stern *et al.* 1984a). The fluvial deposits of the highest terrace are folded and faulted, showing cumulative displacements of *c.* 11 m. Striae on *c.* east-west striking reverse fault planes and on imbricate cobbles are compatible with a subhorizontal  $\sigma_1$  trending N338°E. Shortening directions, as obtained from drag folds, are consistent with a NNW compression (Fig. 9.21).

**Mina El Teniente (34°S).** A systematic study of recent deformation was undertaken at the El Teniente mine, located in the main range. The main source of fault-slip data was a 2.8 to

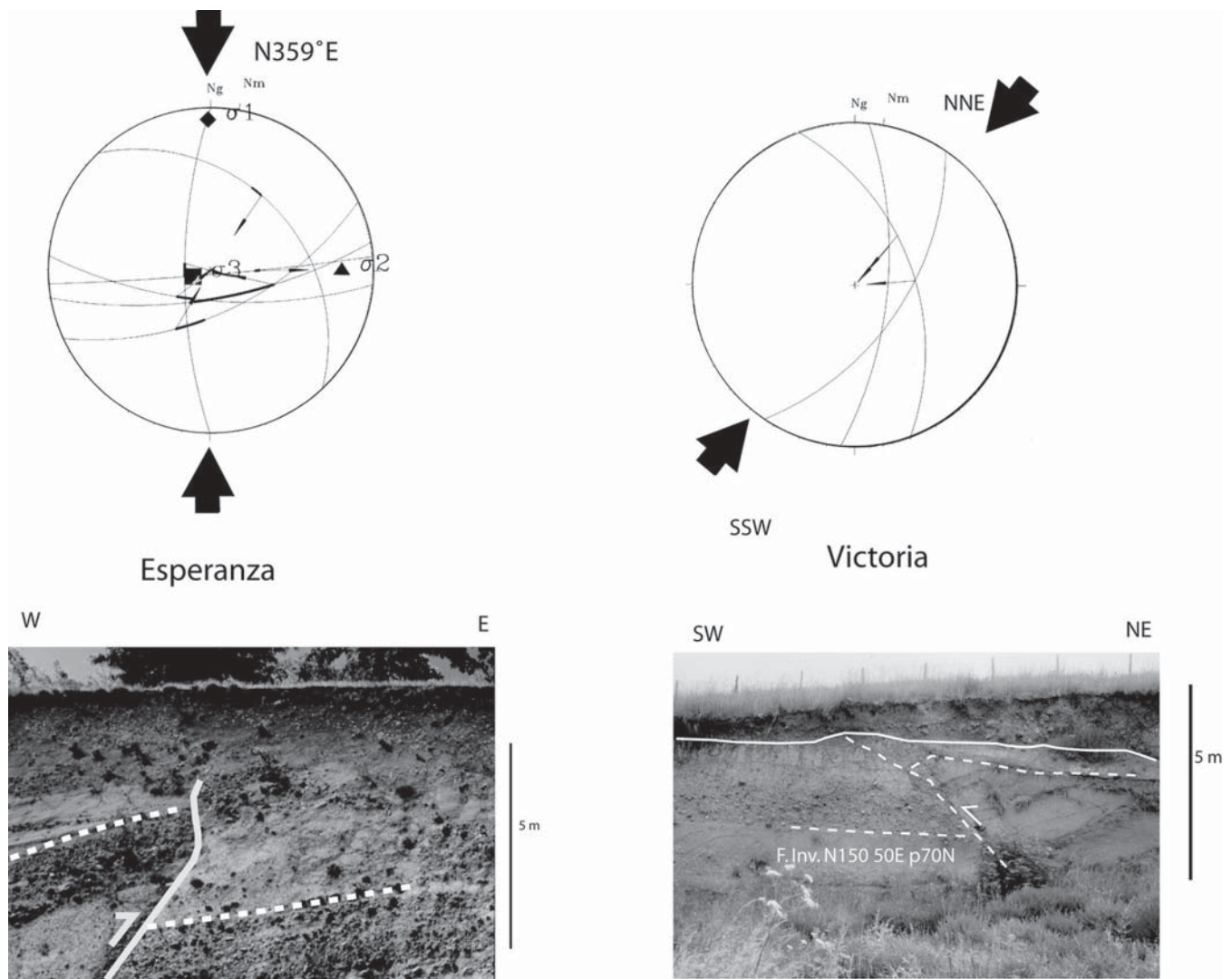


**Fig. 9.20.** Pleistocene sediments in Esperanza and Victoria (37°S) are affected by east–west striking reverse faults, compatible with a north–south to NNE–SSW compressional stress regime.

3.9 Ma lamprophyric dyke, which occurs inside and outside the mine (Cuadra 1986). Twenty-eight mesoscopic striae-bearing faults measured in the lamprophyric dyke are compatible with subhorizontal principal stress directions  $\sigma_1 = N23^\circ E$  and  $\sigma_3 = N293^\circ E$ , respectively. This strike-slip stress tensor is believed to be Pleistocene. Thirteen mesoscopic striae-bearing faults measured in the Braden Breccia are compatible with  $\sigma_1 = N180^\circ E$  (Fig. 9.22).

**Laguna del Laja–Lonquimay–Copahue (37°S).** Folguera *et al.* (2005) recognized a set of post-5 Ma NE and ENE faults making up a transtensional imbricate fan structure which is spatially associated with Recent volcanism. The LOFZ merges north into the Antinir transpressional fault system in Argentina, which represents the present-day active tectonic front of the Andes between 38°S and 39°S latitude (Fig. 9.13).

*Southern segment between 39°S and 46°S: Coastal Cordillera*

There is a complete lack of published field data on the geometry and kinematics of Pleistocene deformation along the Coastal Cordillera at these latitudes. Our limited regional observations suggest that this part of the forearc has accommodated little if any Pleistocene deformation. This is somewhat surprising considering that this region corresponds well to that affected by the great 1960 Valdivia earthquake.

*Southern segment between 39°S and 46°S: Central Valley*

**Fresia–Nueva Braunau (40°S).** Although at 40°S no important lineaments are observed as marking the boundary between the Coastal Cordillera and the Central Valley, sediments in the latter contain evidence for a mid- to late Pleistocene NNE-trending compression event. Mid-Pleistocene fluviglacial sediments, coeval with the Quilleco Polygenetic cone deposits (Thiele *et al.* 1998), are affected by a weak but significant deformation. Fault striae present on pebbles and cobbles are compatible with a subhorizontal compression ranging from N204°E to N26°E at Fresia and N48°E at Nueva Braunau yielding a NNE-trending average compression direction (Fig. 9.23).

**Ancud–Lajas (41°S).** Pleistocene fluviglacial sediments occurring at Chiloe Island, similar to those found at Fresia and Nueva Braunau, also are deformed and faulted. Thirty mesoscopic faults were measured at two sites (Ancud 1 and 2) belonging to a Pleistocene moraine deposit dated as younger than  $0.76 \pm 0.21$  Ma (Vergara & Munizaga 1974). The analysis of ten faults at Ancud 1 yielded a principal stress direction  $\sigma_1 = N17^\circ E$ , with a horizontal  $\sigma_3 = N280^\circ E$ ; Ancud 2 site, with 20 faults, gave a principal stress direction  $\sigma_1 = N29^\circ E$  (Fig. 9.24A,B). Eight faults affecting a  $25.6 \pm 0.7$  Ma ignimbrite (Stern & Vergara 1992) at Ancud 3 are compatible with a horizontal compression  $\sigma_1 = N156^\circ E$  (Lavenue & Cembrano



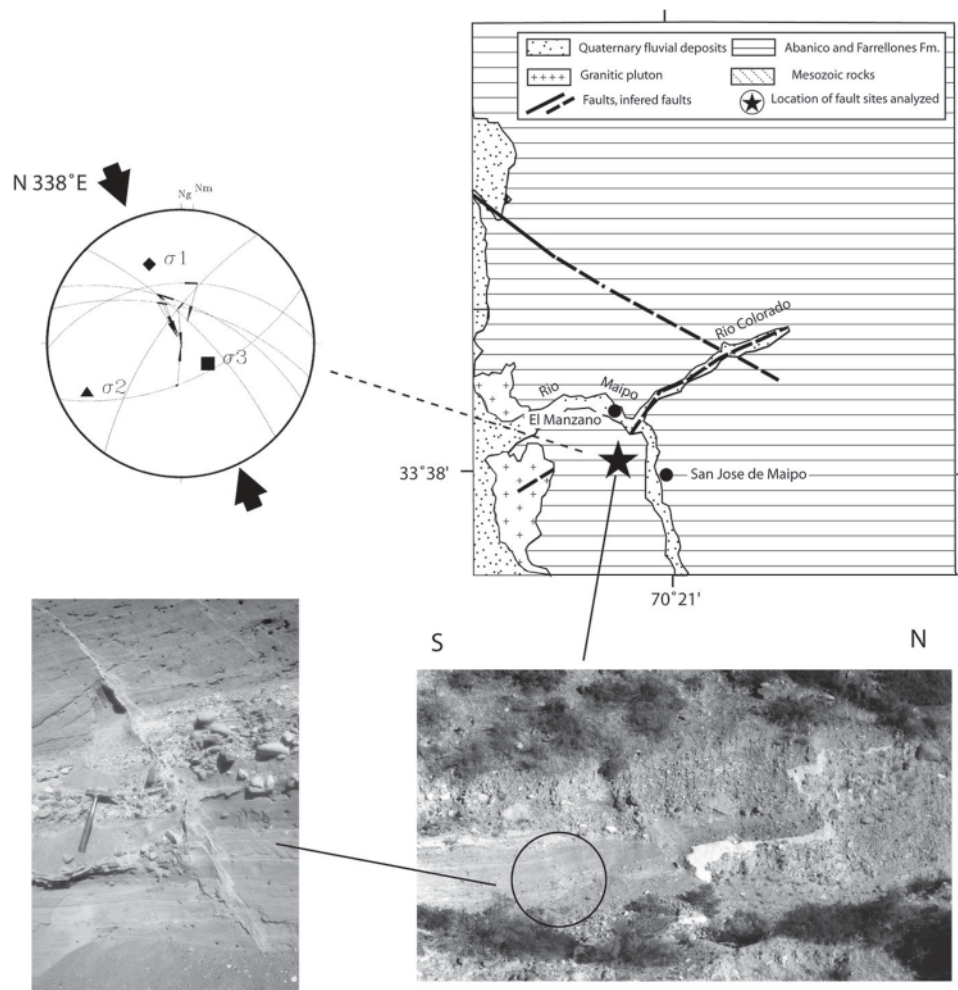


**Fig. 9.21.** Near San José de Maipo (34°S), the fluvial deposits of the Quaternary highest terrace are folded and faulted with a reverse separation of c. 11 m. Striae on c. east–west striking reverse fault planes and on imbricate cobbles are compatible with a subhorizontal  $\sigma_1$  trending N338°E.

1999b). At Lajas site (Fig. 9.24C), the same Pleistocene sediments show faults and striae compatible with  $\sigma_1$  = N341°E (Lavenue & Cembrano 1999b).

#### *Southern segment between 39°S and 46°S: Main Cordillera*

**Liquiñe (39°S).** According to Rosenau (2004), results from drainage network anomalies around Liquiñe are consistent with lineament analysis for the same area highlighting the importance of north–south to NE–SW subvertical fracture zones in the tectonic development of the region. The latter structures have been interpreted by López-Escobar *et al.* (1995a) and Rosenau (2004) as tension cracks spatially associated with Pleistocene volcanism. Furthermore, the N55–60°E orientation of volcanic features would reflect the direction of the main principal stress  $\sigma_1$  in the southern Andes intra-arc zone.

**Cuesta Los Añiques and Lago Caburgua (39°S).** A 8.1 Ma granite exposed in a quarry along one of the main lineaments of the LOFZ exhibits numerous NNE-striking right-lateral faults and ESE-striking left-lateral faults compatible with subhorizontal principal stresses  $\sigma_1$  = N238°E and  $\sigma_3$  = N147°E (Fig. 9.25A). This stress tensor may represent a post-Pliocene dextral transpressional deformation along the LOFZ that is also well documented farther south. Another fault population, made up of NNE-striking normal–left-lateral faults are in turn compatible with a different, extensional stress tensor with NE-trending  $\sigma_3$ . The age and significance of this deformation is

unknown, but may be related to the development of the Central Valley at this latitude. Major NNE-trending and ENE-trending lineaments of the LOFZ cut an 8.5 Ma granodiorite along the eastern margin of Lago Caburga. There, the great majority of mesoscopic faults show strike-slip kinematics, yielding a N228°E-trending  $\sigma_1$ . Although the resulting stress tensor is compressional in nature, it is fairly consistent with Pliocene dextral transpression along the LOFZ (Fig. 9.25B).

**Reloncavi and Volcan Apagado (41–42°S).** Farther south, the NNE-trending faulted margins of the Reloncavi fiord define the LOFZ at c. 41°S. Plurimetric to hectometric vertical faults developed on both Cretaceous and late Miocene granites show superposed sets of striae: an early down-dip set and a late, subhorizontal set. Faults striking 040–110° (mainly 60–80°) are left-lateral reverse-slip. Faults striking 325–25° (mostly 10–20°) show right-lateral reverse to normal slip. This fault population is compatible with a N221°E-trending  $\sigma_1$ , interpreted as a Pleistocene event related to dextral displacement along the LOFZ (Fig. 9.26). Reverse faults with decimetric displacement affect semi-consolidated pyroclastic deposits spatially associated with Apagado Volcano (Fig. 9.26). These deposits are attributed to the Plio-Pleistocene ‘Estratos de Contao’ unit as defined by Alarcón (1995). Fault-slip analysis for the stress tensor yields a subhorizontal principal compression direction  $\sigma_1$  trending N212°E. This is consistent with Pleistocene, intra-arc, dextral transpression.

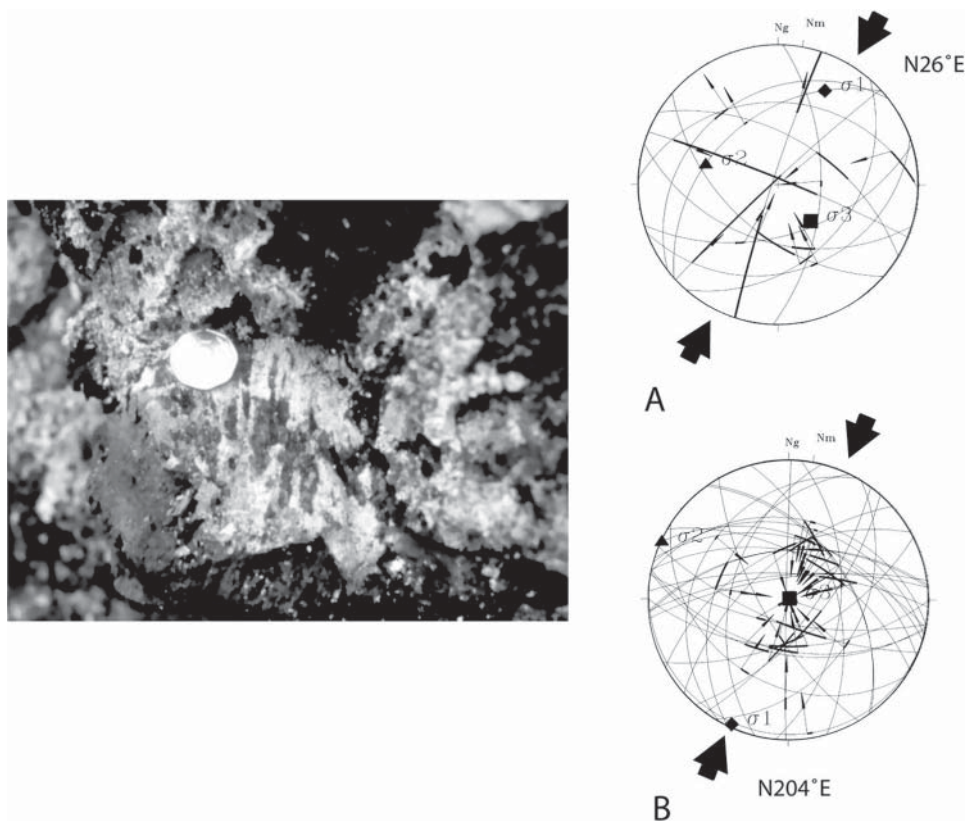


**Fig. 9.22.** Mesoscopic Pleistocene striae-bearing faults measured in the lamprophyric dyke (A) and in the Braden Breccia (B) of El Teniente Mine are compatible with a *c.* north–south subhorizontal principal  $\sigma_1$  stress direction.

**Hornopiren (42°S).** The Cholgo channel, east of Hornopirén, follows the regional trend of the LOFZ at these latitudes (Fig. 9.26). Here, over 50 mesoscopic faults cutting a Pliocene granitoid (3.59 Ma; Schermer *et al.* 1995) yielded a well-constrained subhorizontal principal stress direction  $\sigma_1$  = N236°E (NE–SW) and a subhorizontal  $\sigma_3$  (Fig. 9.26). This stress tensor is compatible with dextral strike-slip displacement on NNE-striking faults of the LOFZ. The fact that Hornopirén Volcano is elongated NE is consistent with Pleistocene to Recent dextral strike-slip deformation of the volcanic arc domain (e.g. Dewey & Lamb 1992).

**Puyuhuapi, Queulat and Puerto Cisnes (44°S).** Miocene diorites and granodiorites cut by Pliocene (3.8 Ma) mylonitic shear zones are exposed along the LOFZ, south of Puyuhuapi (44°S, Fig. 9.26) (Arancibia *et al.* 1999; Cembrano *et al.* 2002). Mesoscopic faults overprint the earlier ductile fabrics and document a dextral transpressional regime with  $\sigma_1$  = N52°E (NE–SW) and  $\sigma_3$  = N321°E (NW–SE) and with  $\sigma_1$  = N211°E (NNE–SSW) and  $\sigma_3$  = N116°E (WNW–ESE). This deformation post-dates a 1.6 Ma cooling age for biotite from a granodioritic unit (Cembrano 1998; Lavenu & Cembrano 1999b) and so can be considered as Pleistocene. The direction of the maximum horizontal stress is subparallel to an elongated cluster of monogenic alkaline volcanoes, suggesting that dextral transpression is still active (López-Escobar *et al.* 1995a).

In the southern part of the Andes, and along the Liquiñe–Ofqui Fault Zone (Fig. 9.17), published fault-slip data for the intra-arc region between 39°S and 47°S indicate that the state of stress was transpressional, with  $\sigma_1$  orientated in a NE–SW direction. The Pleistocene transpressional deformation has been dated as younger than 1.6 Ma (Lavenu & Cembrano 1999b). Partitioning of deformation is recorded along and

across the western continental margin between 33°S and 47°S (Fig. 9.27). Horizontal compression trending north–south to NNE–SSW has affected the Quaternary deposits at the coast, in the Central Valley and in the Main Cordillera, and McKinnon & Garrido de la Barra (2003) have also observed the north–south trending shortening as Quaternary. The intra-arc zone, where the LOFZ is located, has been affected by NE–SW transpressive deformation with dextral movement along the main fault zone. This north–south to NE–SW deformation has been dated as after 2.4 Ma in the Santiago region (33°S), after  $0.76 \pm 0.21$  Ma in Chiloe Island (43°S) (Vergara & Munizaga 1974) and after 1.6 Ma in the Puyuhuapi area (45°S). To the east of the LOFZ, the remainder of the Cordillera and the Argentinian Subandean zone have little or no evidence of Quaternary deformation (Diraison *et al.* 1998). Recent contributions (Melnick *et al.* 2002; Folguera *et al.* 2004) suggest the continuation of the northernmost trace of the LOFZ into the eastern Andean hillslope between 37°S and 38°S, through the Antñir–Copahue Fault, where Quaternary activity and gravity-related phenomena have been reported. Thus, the LOFZ seems to accommodate much of the upper plate deformation, with no significant deformation after the middle Miocene recognized in the Argentinian Subandean zone between 33°S and 52°S (Costa *et al.* 2000a; Cembrano *et al.* 2002).

#### **Relationship between neotectonics and seismicity for central and southern Chile**

Previous studies have shown that the subducted oceanic Nazca Plate beneath South America exhibits strong along-strike variations in the dip angle that suggest segmentation of the downgoing slab (Barazangi & Isacks 1976; Cahill & Isacks



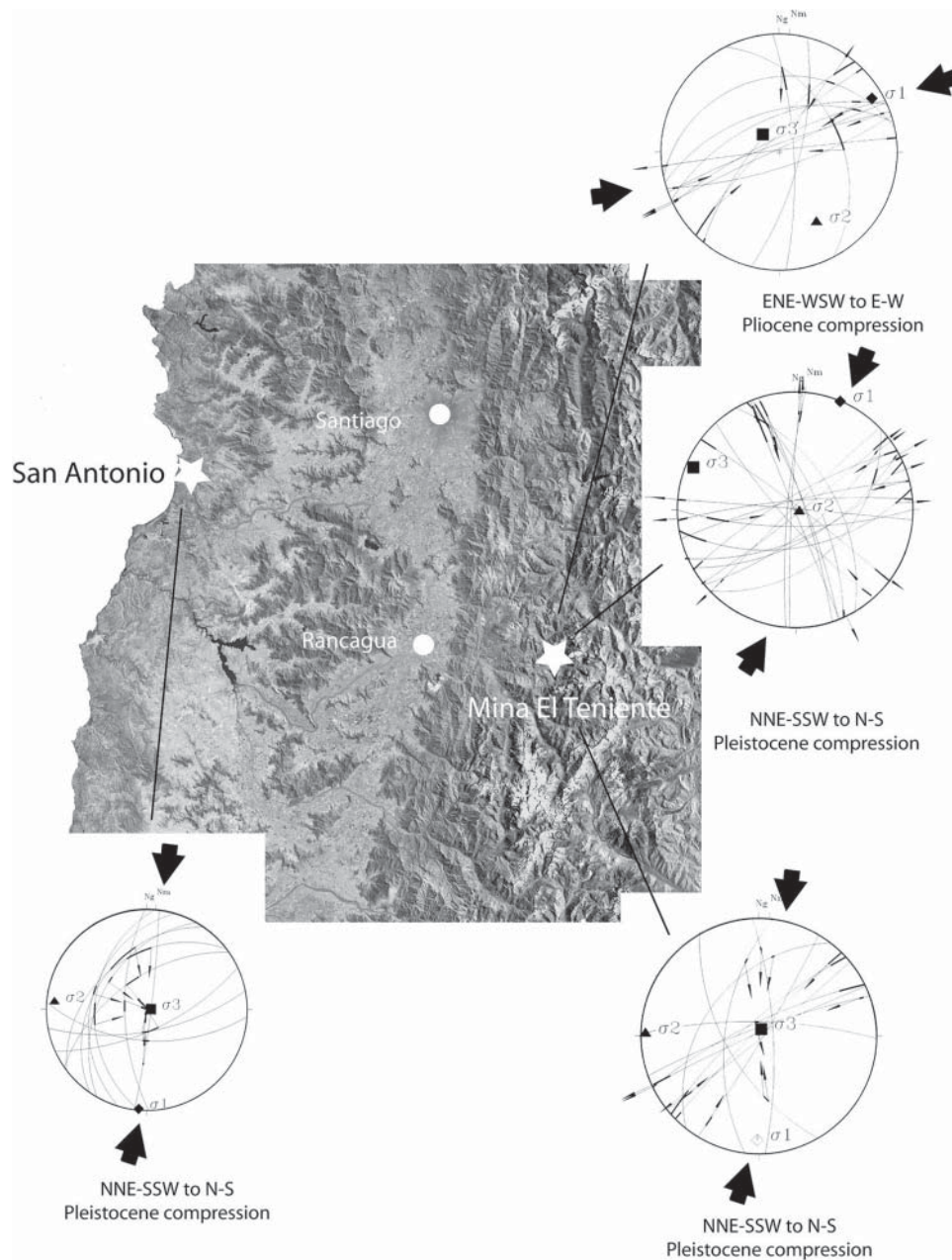


Fig. 9.23. Pleistocene compression recorded in gravel deposits of the 'Rodados Multicolores' in the Central Depression close to Fresia (40°S).

1992). The shape of the Nazca Plate beneath central Chile, which is inferred from the top of the local and teleseismically recorded seismicity in the zone, shows a sharp transition around 32–33°S from subhorizontal slab to the north to a 27°-dipping slab at intermediate depths to the south. The central Chile subduction zone is very seismically active, with magnitude 8 interplate thrust earthquakes having occurred historically along its entire length (Comte *et al.* 1986; Beck *et al.* 1998). The zone between 31°S and 33°S has been the nucleation site for several large thrust events (e.g. 1944,  $M_s=7.4$ ; 1971,  $M_s=7.5$ ; 1977,  $M_s=7.4$ ; 1985,  $M_w=8.0$ ), intraplate events below the subduction interface, and events within the subducted slab (1965,  $M_s=7.5$ ). The Punitaqui earthquake of 15 October 1997 ( $M_w=7.1$ ) is an example of an intraplate earthquake in the flat-slab zone (Pardo *et al.* 2002b).

South of latitude 32–33°S, the slab steepens in dip from nearly 10° to 25–30° (Pardo *et al.* 2002a). Based on teleseismic and local data, Barazangi & Isacks (1976) proposed that this

change in dip is accommodated by a tear in the slab or by a continuous southward flexure or ramp. More recently Cahill & Isacks (1992) have proposed a continuous flexure as the transition between the flat-slab to the north and the steep subduction zone to the south of 33°S.

The great San Antonio–Valparaíso earthquake ( $M_s=7.8$ ) in central Chile occurred on 3 March 1985. Fault slip was concentrated at a depth between 30 and 40 km within the interplate zone and induced coseismic coastal uplift (Comte *et al.* 1986; Barrientos 1988). There is no field evidence for reactivation of surface faults as a result of this relatively deep crustal earthquake.

In south-central Chile, Campos *et al.* (2002) document shallow earthquakes beneath the Andean volcanic chain. In the Central Valley, two events that were located at depths of 28 and 42 km on N20–30°E faults are puzzling. Their focal mechanisms are compatible with a northward displacement of the Coastal Cordillera block relative to the Central Depression.

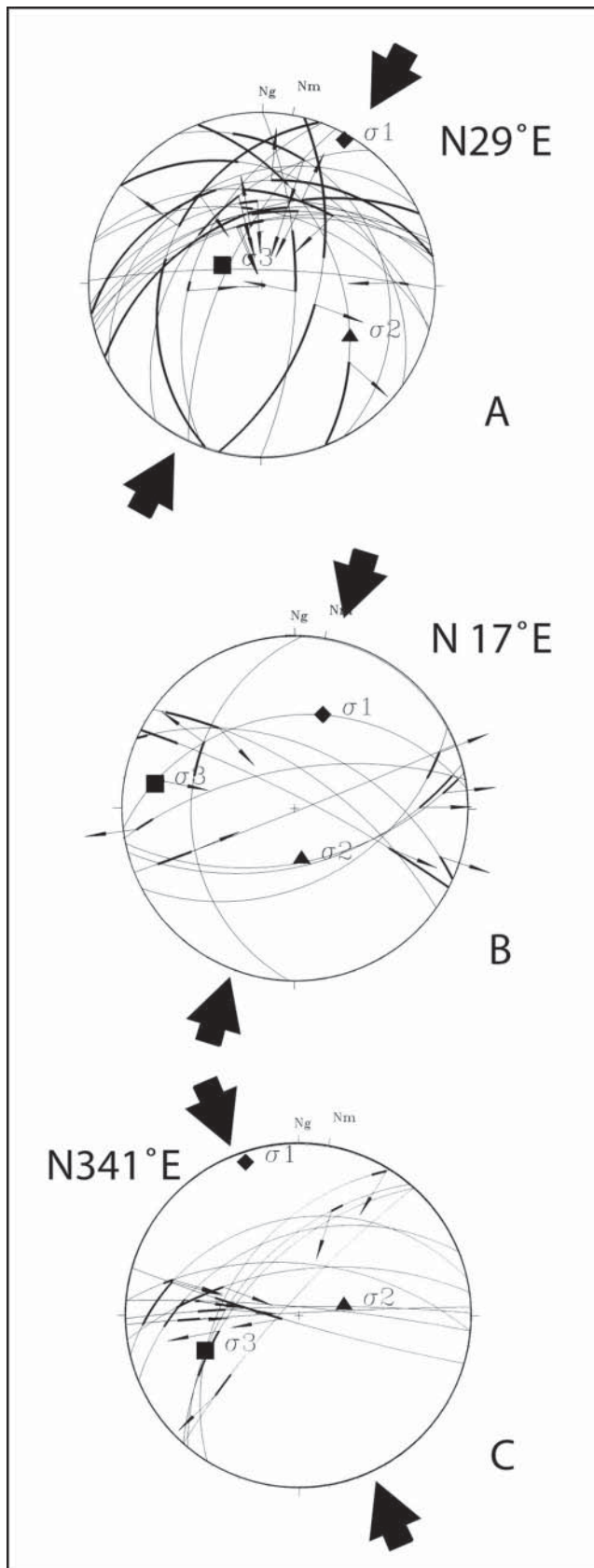


**Fig. 9.24.** Stereoplots of Pleistocene faults and striae in glacial deposits and volcanic rocks of the Central Valley close to Ancud, Chiloé Island (42°S): moraine deposits (A and B) and ignimbrite (C). Inversion of fault-slip data for the stress tensor, consistently show a NNE to NNW trending subhorizontal  $\sigma_1$ .

These displacements are consistent with well documented compressional to transpressional deformation associated with north–south to NNE-trending compression in the Central Valley and volcanic arc, respectively. This in turn suggests that the roughly north–south coseismic deformation need not be compatible with the interseismic east–west deformation indicated by GPS data.

After the Lonquimay/Navidad crater erupted on 25 December 1988 in southern Chile (38°S), seismicity increased over the next few days (Barrientos & Acevedo 1992). According to these authors, the largest shallow crustal event ( $M_w=5.3$ ) of the series took place on 24 February 1989, at between 6 and 10 km depth. The focal mechanism corresponded to a right-lateral compressive (transpressional) strike-slip fault that coincides with the strike of the Liquiñe–Ofqui Fault Zone. This focal mechanism shows a NE–SW to NNE–SSW trending compressional stress axis that corresponds to the Quaternary surface transpressional stress documented by hectometric to kilometric faults in the field.

The largest earthquake recorded in the world was the great Valdivia earthquake of 22 May 1960 (Pflafer & Savage 1970), which was estimated at  $M_s=8.5$  (minimum) and  $M_w=9.4$ . The earthquake occurred along the subduction interface thrust zone (25 km depth, 1000 km length rupture, 200 km down-dip width, and displacement of 20–40 m) and produced coseismic vertical displacement (warping uplift and subsidence) in the coastal zone. No precise focal mechanism was available at the time of the earthquake. There is no convincing evidence for surface fault activity associated with this or other subduction interface earthquakes in historic times. According to Pflafer & Savage (1970), the southern part of the Central Valley, between 38°S and 46°S, experienced post-seismic deformation, mainly vertical displacements.

In southern Chile, Chinn & Isacks (1983) reported a teleseismically recorded shallow crustal earthquake near the Hudson Volcano (46°S, 73°W) on 28 November 1965. With a depth of 33 km and  $M_s=6$ , this earthquake could have occurred on a NNE–SSW trending right-lateral fault that would belong to the right-lateral Liquiñe–Ofqui Fault Zone, which is located about 25 km to the west. This earthquake is consistent with our neotectonic observations along the LOFZ. Further south, in Laguna San Rafael (46.75°S, 73.90°W), sag ponds and dextral strike-slip indicators along reactivated fault planes are compatible with the NE–SW transpression documented elsewhere.

### Discussion

Published analyses of fault-slip data show that the stress field in many areas throughout the central and southern Andean forearc switched from widespread Pliocene east–west compression to Pleistocene north–south compression or north–south and east–west extension near the Pacific coast. In contrast, the state of stress in the backarc above the flat-slab zone (Sierras Pampeanas in Argentina) has remained compressional and east–west during Pliocene and Pleistocene times. These differences in regional stresses cannot be easily accounted for by plate kinematics alone because, along the central Andes, the convergence vector has not changed significantly during the past 6 Ma. Furthermore, when considering the whole Andean chain from forearc to backarc regions, different regions record different stress fields during both the Pliocene and Pleistocene as a function of the distance from the trench, slab geometry and topography. Which then are the processes responsible for the nature and spatial distribution of these different tectonic regimes?

On the Pacific Coast, the east–west trending extension is the most recent deformation observed, and it corresponds to the elastic rebound of the continental plate edge after large subduction interface earthquakes. Displacement results from two



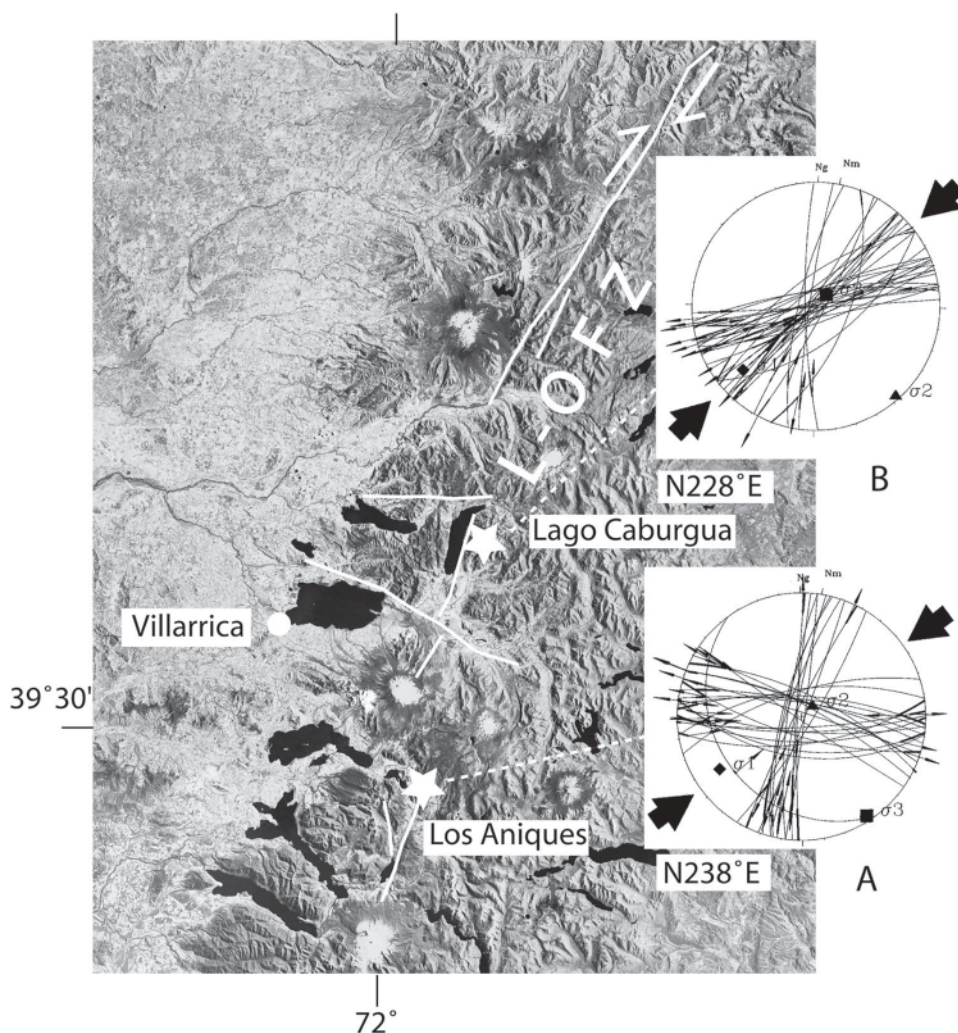


**Fig. 9.25.** Fault-slip data and stress tensor for Pleistocene deformation along the northern portion of the LOFZ at Los Aniques (A) and Caburga (B). A subhorizontal  $\sigma_1$  trending NE–SW is compatible with right-lateral displacement along the LOFZ.

deformation processes: (1) interseismic accumulation of elastic strain in relation to the subduction coupling; and (2) coseismic strain release during the earthquake.

How can we explain that in the central and southern Chile forearc the compressional direction became north–south? The following processes can account for the north–south compression: (1) strike-slip partitioning arising from oblique convergence favours a potential northward displacement gradient of a forearc sliver against a buttress producing north–south shortening (e.g. Beck *et al.* 1993); (2) forearc northward motion is enhanced by the collision of successive portions of the Chile Ridge; (3) the kinematics of the forearc deformation depends on the geometry of the plate boundary and the convergent margins concave towards the subducting plate, thus causing margin-parallel shortening as a ‘buttress effect’ (Beck 1991; McCaffrey 1992, 1996; Allmendinger *et al.* 2005); and (4) another ‘buttress effect’ can also be the abrupt shallowing in the slab dip from 30° south of 33°S to subhorizontal north of 33°S. Allmendinger *et al.* (2005) also show good evidence of Neogene trench-parallel shortening in the forearc of northern Chile. In their interpretation, margin-parallel shortening arises from a north–south elastic velocity gradient at a locked, curved plate boundary, as modelled by Bevis *et al.* (2001). As a comparison, in North America, Johnson *et al.* (2004) have similarly interpreted the north–south margin-parallel shortening of the

Cascadia forearc to be a consequence of oblique (NE–SW) subduction of continental and oceanic plates at a curved margin.

Subduction of oceanic ridges does not appear to induce long-term regional compressional deformation, but rather enhances continental margin uplift. There is no conclusive evidence of more significant or widespread deformation under compression above subducted oceanic ridges: during the Pliocene, for example, compression along all the active margin of the Andes was orientated east–west.

Deformation caused by ridge subduction is observed close to the trench and is associated with an increase in the seismic activity at the subduction zone. Different types of deformation in the trench sedimentary fill and/or in the accretionary wedge are observed with or without seismic activity such as in the Andes, Marianas and Costa Rica (Cloos & Shreve 1996; von Huene & Ranero 2003).

The coastline above a subducting ridge shows a significant increase in surface uplift. This is the case for the Nazca Ridge, above which Quaternary and Pliocene marine terraces and their deposits are uplifted to high altitudes not seen in any other part of the Pacific coast of South America. The 125 ka marine terraces (MIS 5) are as high as 105 m a.s.l. and the Pliocene terraces reach altitudes of 780 m a.s.l. (Ortlieb & Macharé 1990) (Fig. 9.28).

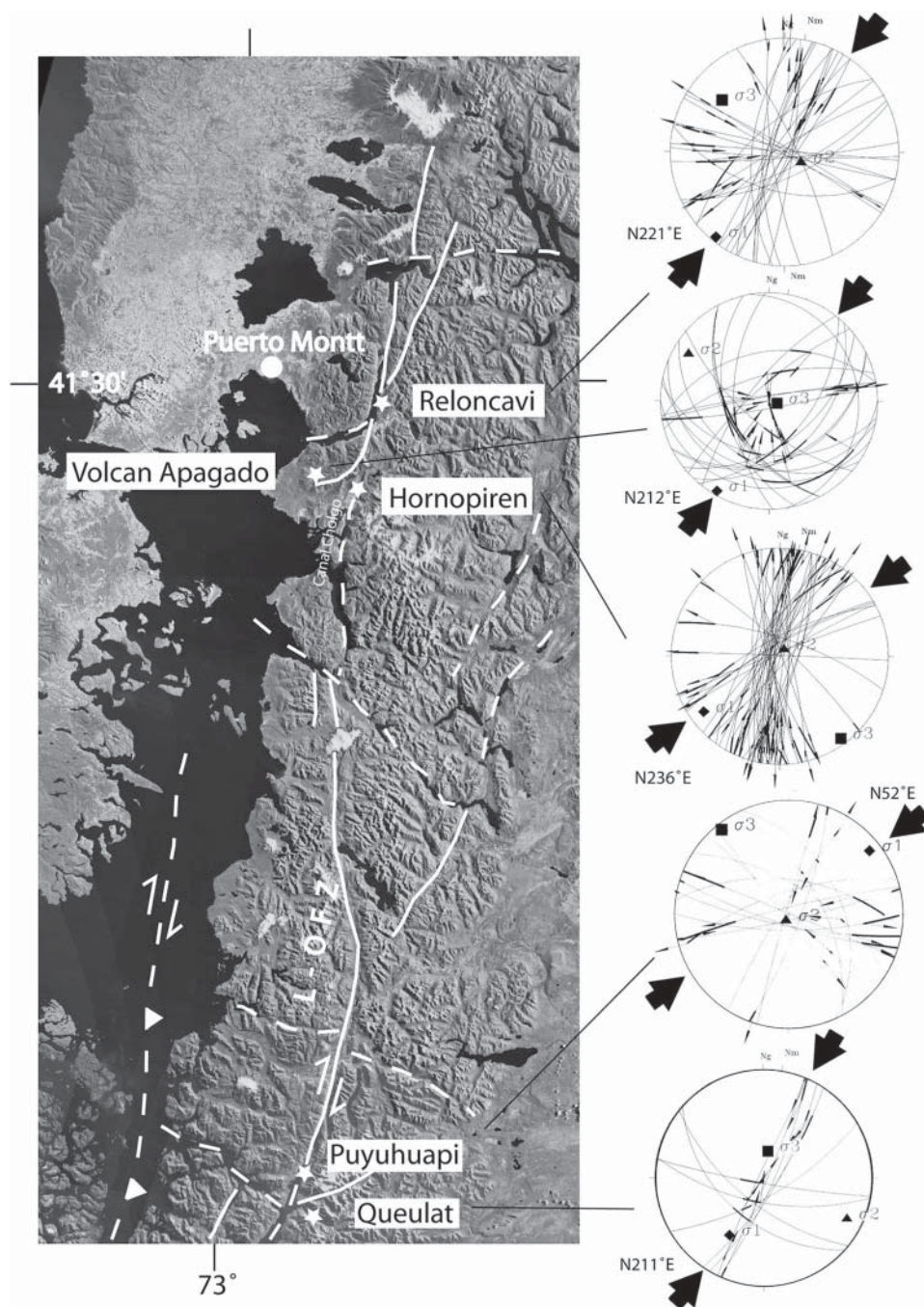


**Fig. 9.26.** Fault-slip data and stress tensor for Pleistocene deformation along the central and southern portion of the LOFZ. A subhorizontal  $\sigma_1$  trending NE–SW is compatible with right-lateral displacement along the LOFZ.

Near latitude 33°S, the Juan Fernandez Ridge deforms the thinned crust at the continental margin and inland through the forearc, volcanic arc and backarc. According to von Huene *et al.* (1997) it is difficult to correlate existing tectonic structures on the overriding plate with the arrival of the ridge; instead they relate it to previous tectonic events, although other authors have proposed otherwise (Yañez *et al.* 2002). There is no evidence of uplifted Quaternary marine terraces on the continental margin affected directly by the predicted subduction of the Juan Fernandez Ridge. On the contrary, a few degrees to the north, in La Serena–Altos de Talinay and Caldera, Quaternary marine terraces have been uplifted as much as 200 m a.s.l. without an oceanic ridge being subducted. Similarly, over other oceanic ridges or seamounts worldwide, no significant uplift is noticed

at the forearc region. Generally the coastal zone uplift has marine terrace heights which could be classified as ‘normal’, with a MIS 5 terrace at 25 to 30 m a.s.l. and the upper Quaternary terraces at 200 m a.s.l.

After 22–25 Ma, DeMets *et al.* (1990) and D. E. Engebretson (pers. comm. 1995) indicate slight increases within an overall slowdown in the convergence rate at 4.9 Ma in the early Pliocene, and near 2 Ma in the latest Pliocene. On the contrary, during the same time, Somoza (1998) indicates a slowdown in the convergence rate which is coeval with a global event during early Pliocene times and with an east–west trending compression that affected the whole mountain range. After 2.4 Ma another, less intense global change affected the chain in a differential way, yet corresponds to Engebretson and DeMets



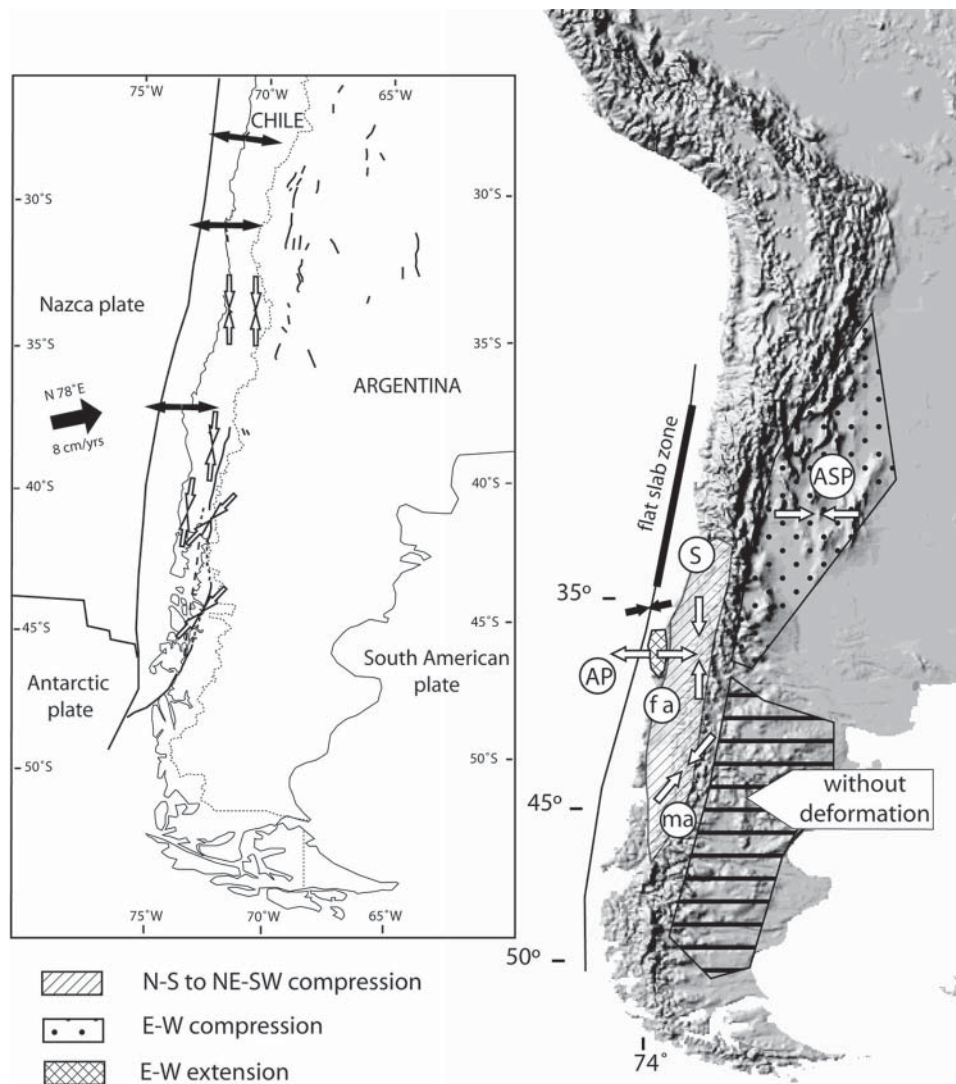


**Fig. 9.27.** Summary figure showing the results of the microtectonic analysis of Pleistocene faults from central and southern Chile and other parts of the Andes, for comparison. East–west extension is recorded along the Pacific Coast, at the Arauco Peninsula; north–south to NE–SW compressive and strike-slip regimes are documented in the forearc and the intra-arc zones in Chile; east–west compressional tectonic regime in the Argentinian central foreland (SE of Sierras Pampeanas) (e.g. Bettini 1980; Costa *et al.* 2000b).

models. In effect, there are changes in the recorded stress field in Chile as follows: after 5.5 Ma (Puerto Cisnes), 4.0 Ma (Mina El Teniente), 2.4 Ma (Mina El Teniente) and, during the Pleistocene, after 1.6 Ma (Puyuhuapi) and middle Quaternary (Chiloé).

### Short-term upper plate deformation: GPS data

One key question in neotectonics is how long-term and short-term deformation data can be reconciled. For instance, it seems reasonable to compare the recent stress field obtained from fault-slip data with that implied by modern GPS measurements. Published GPS data concerning deformation above the Nazca–South America plate boundary in the central Andes consistently show west–east velocity vectors that are nearly parallel to the convergence vector (Norabuena *et al.* 1998; Bevis *et al.* 1999, 2001; Kendrick *et al.* 1999, 2001; Klotz *et al.* 2001; Brooks *et al.* 2003). These authors interpret these displacements as the result of the interseismic crustal velocity field. During large subduction earthquakes, slip along the plate interface induces

coseismic east–west extensional deformation in the upper plate, roughly parallel to the slip vector convergence (Fig. 9.18). This was the case for the 1960 southern Chile earthquake (Plafker & Savage 1970; Barrientos & Ward 1990) and the 1995 Antofagasta earthquake (Delouis *et al.* 1998), both of which were located in the outer forearc in the western Coastal Cordillera area. Another paper (Ruegg *et al.* 2002) interprets the N89–90°E GPS-derived velocity vectors relative to stable South America as reflecting interseismic strain accumulation above the Nazca–South America subduction zone.

Following Delouis *et al.* (1998) we assume that the interseismic compression in the overriding plate is due to the plate motion, while the plate interface is locked at shallow depth, as illustrated in Bevis & Martel (2001). Therefore, within the southern forearc of Chile, we can interpret the north–south neotectonic compression deduced from microfault analysis to be the result of coseismic deformation, orientated perpendicular to the slip vector and due to the partition of deformation inside the forearc and along its edge with the backarc region (Fig. 9.19). The focal mechanisms reported by Campos *et al.* (2002) appear to support this interpretation.

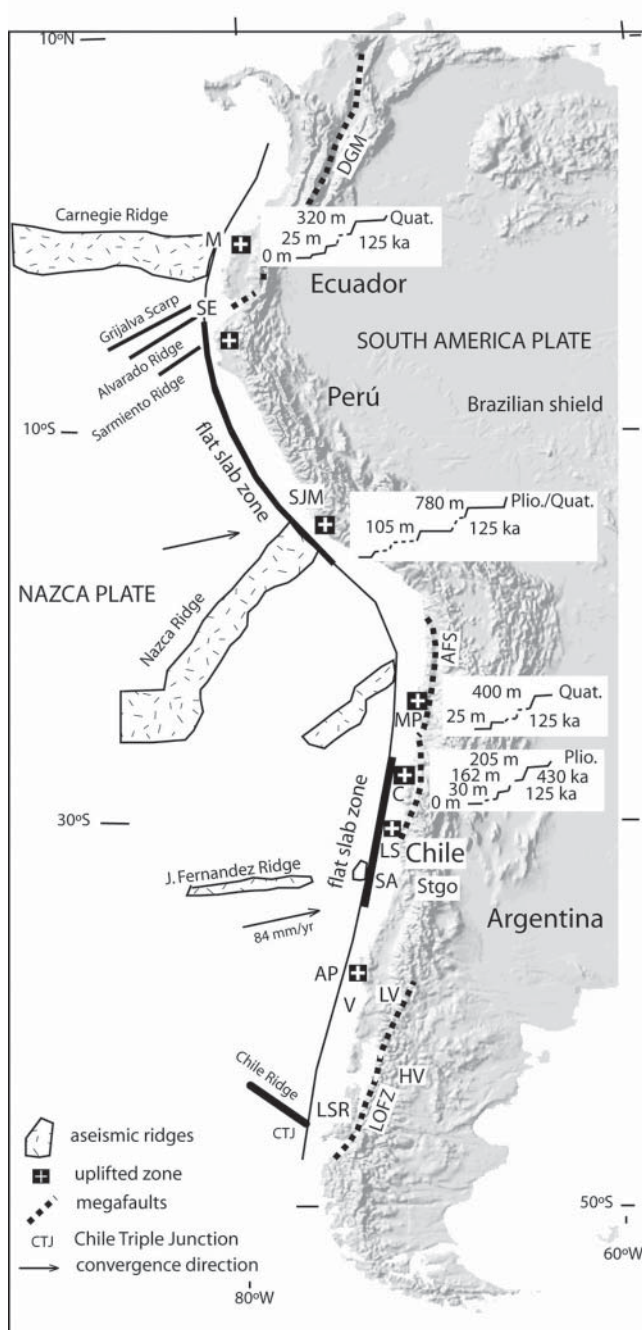


**Fig. 9.28.** Small topographic sections show coastal uplift from Ecuador, Peru, and Chile. Abbreviations: AFS, Atacama Fault System; AP, Arauco Peninsula; C, Caldera; CTJ, Chile triple-junction; DGM, Dolores–Guayaquil Megashear Fault System; HV, Hudson volcano; LOFZ, Liquiñe–Ofqui Fault Zone; LS, La Serena; LSR, Laguna San Rafael; LV, Lonquimay volcano; M, Manta; MP, Mejillones Peninsula; SA, San Antonio; SE, Santa Elena; Stgo: Santiago; V: Valdivia.

In the southern part of the central Andes (central and southern Chile) we suspect that the slip partitioning into the forearc corresponds to the development of a forearc sliver (Fig. 9.29) as proposed in the model of Fitch (1972), with the LOFZ being the limit between the forearc and the backarc region of the South American Plate.

Bevis *et al.* (2001) and Bevis & Martel (2001) regard the Andean Cordillera as a rigid microplate located between Nazca and South American plates. In fact, in the middle and southern parts of the central Andes, one cannot consider this really a

rigid portion because it is cut into several thin slivers, parallel to the trench and the main direction of the Cordillera. The partitioning of Cenozoic deformation was achieved along several principal right-lateral reverse faults that trend N10°E, and form a transpressional flower structure (Fig. 9.29) (Cembrano *et al.* 2002). This slip partitioning could correspond in part to a ‘smoothly distributed plastic’ deformation within ‘a mechanically coherent forearc’ as in the Bevis & Martel (2001) model, but the lack of structural or offset stratigraphic markers does not allow us to determine the amount of displacement along the LOFZ and within the forearc slivers.

In a recent article, Allmendinger *et al.* (2005) have demonstrated that interseismic elastic deformation and permanent deformation show surprisingly similar spatial and temporal patterns. In particular, the sense and amount of long-term block rotations in the central Andes Bolivian Orocline, as revealed by palaeo-magnetic data are consistent with the instantaneous picture given by GPS data when extrapolated in time. Consistency between elastic and permanent deformation would reflect that both types of deformation are driven by the same stress field.

## Conclusions

Neotectonic studies along and across the central and southern Chilean Andes document a number of different tectonic regimes during Pliocene and Quaternary times. Extensional, compressional, transpressional and transtensional deformations are each recorded in various morphostructural zones and several mechanisms are proposed to explain these tectonic changes in time and space. Because we have access only to surface faults, the local analysis of fault-slip data does not necessarily reflect the general state of stress of the Cordillera which has been under a relatively constant convergence regime for the past 10 Ma, both in magnitude and direction. However, there is a clear regional pattern to stress fields that are well correlated with major tectonic domains such as the forearc, volcanic arc and foreland.

1. Segments of the coast, close to the trench, are mostly affected by east–west trending extension, a consequence of the elastic rebound of the upper plate which is subjected to uplift and westward displacement during and after compressional earthquakes of the subduction interface zone. Alternatively, outer forearc extension can be attributed to interseismic folding and associated stretching of the surface (e.g. González *et al.* 2003; Allmendinger *et al.* 2005).
2. Inside the forearc zone, farther away from the trench, a weak but well documented north–south compression (i.e. central and southern Chile) results from coseismic deformation partitioning of oblique convergence and a concomitant northward lateral displacement gradient of the forearc block against a transversal buttress (i.e. the heterogeneity on the subducting Nazca Plate near latitude 33°S). There is still little evidence of Plio–Quaternary surface deformation in the inner forearc of northern Chile.
3. The Andean intra-arc zone between 39°S and 46°S has undergone NE–SW transpression (Liquiñe–Ofqui Fault Zone) as a consequence of coseismic and/or interseismic deformation partitioning.
4. The Andean orogenic front above the Pampean flat-slab and the Sierras Pampeanas undergoes east–west compression with a variable strike-slip component, although local north–south compression during the Quaternary cannot be ruled out.
5. Current GPS data showing periods of interseismic shortening parallel to the convergence vector and coseismic extension are only partly compatible with actual structures observed in the field. Only the outer forearc shows evidence of coseismic crustal extension; the inner forearc does not record significant deformation amenable to interseismic



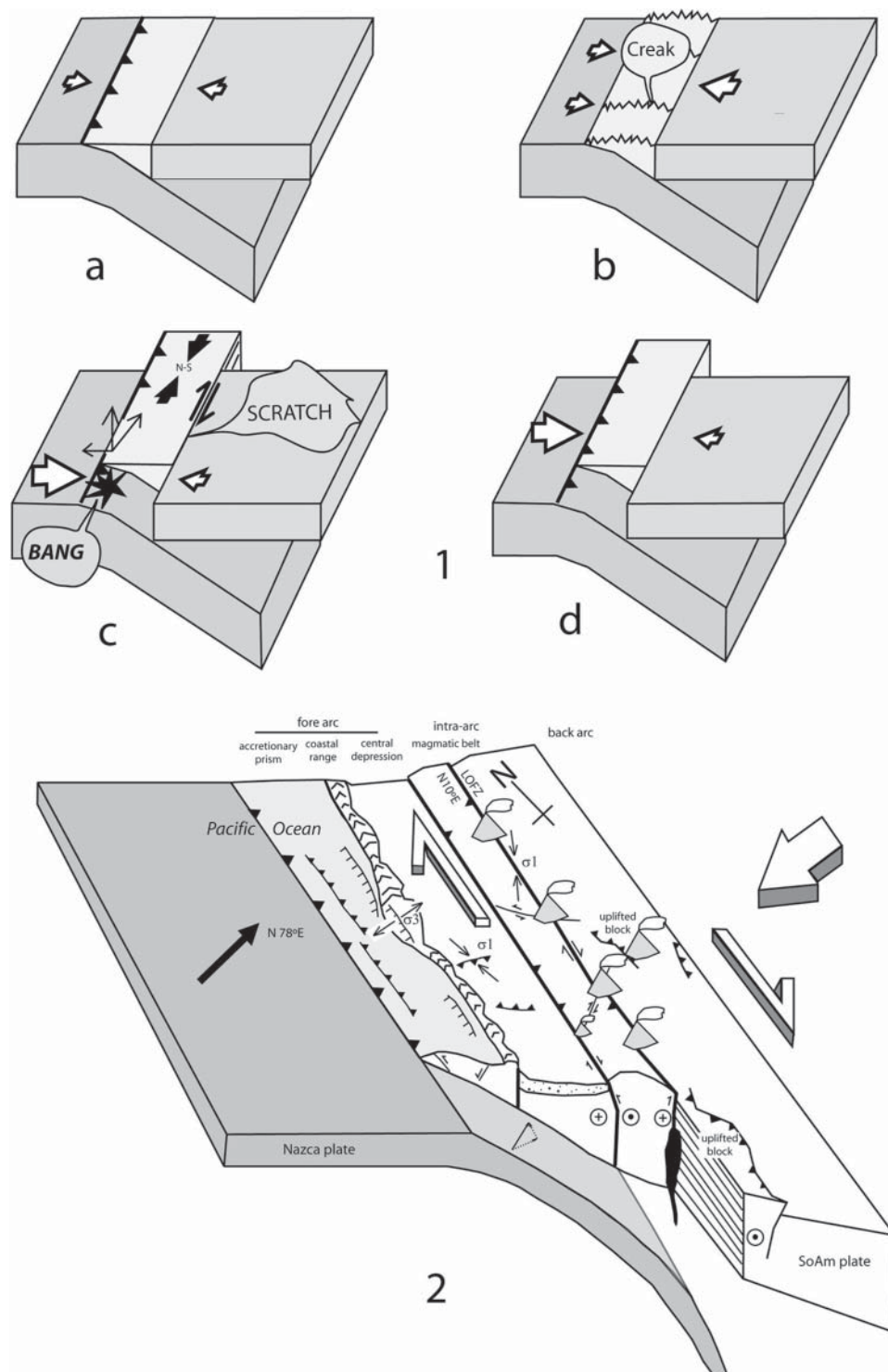


**Fig. 9.29.** Kinematic partitioning of oblique plate convergence. 1, Geocartoons showing three states of the deformation of the active margin (a) during interseismic (b) and coseismic (c) deformation before normal state (d). 2, Schematic block diagram showing how heterogeneous compressional and transpressional deformation accommodates oblique convergence along and across the plate boundary (state (c) of the geocartoons). Convergence is resolved into east–west extensional deformation in the outer forearc zone, north–south contraction in the inner forearc zone, and transpressional deformation concentrated in the volcanic arc zone. LOFZ, Liquiñe–Ofqui Fault Zone.

east–west shortening. The north–south compression documented in the inner forearc of central–southern Chile can be attributed to coseismic deformation partitioning of oblique convergence.

J.C., A.L., G.G. and G.Y. thank FONDECYT Projects 1931096, 1950497, 1020972, 1020436 and 1040389 for funding their work in Andean Tectonics over the last ten years. Our research has been also

supported by Institut de Recherche pour le Développement (IRD) UR 154 to A.L., ‘Convenio’ IRD–University of Chile, ‘Proyecto Geodinámico El Teniente’ between University of Chile and CODELCO, and the Program ECOS-Sud C00U01 (2000–2003) to A.L. and J.C. Constructive reviews by R. Allmendinger and V. Ramos helped to significantly improve the manuscript. W. Gibbons and T. Moreno are thanked for their kind and timely editorial help throughout the review process. We also thank C. Rojas, who helped to revise the last version of the manuscript.